Cardiac Arrhythmias: What can we learn of Mathematical Models for Cardiac Tissue?

Rahul Pandit

Centre for Condensed Matter Theory

Department of Physics

Indian Institute of Science, Bangalore, 560012

26 June 2018

Dynamics of Complex Systems - Workshop

ICTS-TIFR, Bangalore

Acknowledgements

- Ashwin Pande, Ahmedabad University, Ahmedabad.
- Sitabhra Sinha, Institute of Mathematical Sciences, Chennai.
- TK Shajahan, NITK, Surathkal.
- Alok Ranjan Nayak, IIIT, Bhubaneswar.
- Rupamanjari Majumder, MPI, Dynamics and Self-Organization, Goettingen.
- KV Rajany, Soling Zimik, Mahesh K. Mulimani, IISc, Bangalore.
- Alexander V. Panfilov, University of Ghent, Belgium.

Acknowledgements

Funding and support:

- DST, CSIR, UGC, India.
- Robert Bosch Centre for Cyber Physical Systems, IISc.
- SERC, IISc.

Publications

- Spiral Turbulence: From the Oxidation of CO on Pt(110) to Ventricular Fibrillation - A. Pande, S. Sinha, and R. Pandit , Journal of Indian Institute of Science, Vol. 79, 31 (1999).
- Spatiotemporal Chaos and Nonequilibrium Transitions in a Model Excitable Medium, A. Pande and R. Pandit , Phys. Rev. E, Vol. 61, 6448 (2000).
- Defibrillation via the Elimination of Spiral Turbulence in a Model for Ventricular Fibrillation, S. Sinha, A. Pande and R. Pandit , Phys. Rev. Lett., Vol. 86, 3678 (2001).
- Spiral Turbulence and Spatiotemporal Chaos: Characterization and Control in Two Excitable Media, R. Pandit , A. Pande, S. Sinha, and A. Sen, Physica A, Vol. 306, 211 (2002).
- Ventricular Fibrillation in a Simple Excitable Medium Model of Cardiac Tissue, T.K. Shajahan, S. Sinha, and R. Pandit, International Journal of Modern Physics B, Vol 17, No 29, pp. 5645-5654 (2003).

Publications

- Spatiotemporal chaos and spiral turbulence in models of cardiac arrhythmias: an overview, T K Shajahan, Sitabhra Sinha and Rahul Pandit, Proceedings of Indian National Science Academy, 71, A, pp.47-57 (2005).
- Spiral-Wave Dynamics Depends Sensitively on Inhomogeneities in Mathematical Models of Ventricular Tissue, T K Shajahan, Sitabhra Sinha and Rahul Pandit, Phys. Rev. E, 75, 011929 (2007).
- The Mathematical Modelling of Inhomogeneities in Ventricular Tissue - T.K. Shajahan, S. Sinha and R. Pandit , in Complex Dynamics in Physiological Systems: From Heart to Brain (Eds. S.K. Dana, P.K. Roy and J. Kurths), Springer (2009) pp 51-67. *http://lanl.arxiv.org/abs/nlin.CD/0703048*
- Spiral-Wave Turbulence and its Control in the Presence of Inhomogeneities in Four Mathematical Models of Cardiac Tissue, TK Shajahan, A.R. Nayak, and R. Pandit, PLoS ONE 4(3): e4738 (2009).

Publications

- An Overview of Spiral- and Scroll-Wave Dynamics In Mathematical Models for Cardiac Tissue, R. Majumder, A. R. Nayak, and R. Pandit, invited book chapter, in O.N. Tripathi, U. Ravens, and M.C. Sanguinetti (eds.), Heart Rate and Rhythm, DOI 10.1007/978-3-642-17575-6 14, (Springer-Verlag, Berlin, Heidelberg 2011) Chapter 14, pp 269-282.

- Scroll-Wave Dynamics in Human Cardiac Tissue: Lessons from a Mathematical Model with Inhomogeneities and Fiber Architecture, R. Majumder, A.R. Nayak, and R. Pandit, PLoS ONE 6(4): e18052 (2011).

- Nonequilibrium Arrhythmic States and Transitions in a Mathematical Model for Diffuse Fibrosis in Human Cardiac Tissue, R. Majumder, A.R. Nayak, and R. Pandit, PLoS ONE 7(10): e45040 (2012).

- Spiral-Wave Dynamics in a Mathematical Model of Human Ventricular Tissue with Myocytes and Fibroblasts, A.R. Nayak, TK Shajahan, A.V. Panfilov, and R. Pandit, PLoS ONE 8(9): e72950 (2013).

Publications

- A study of early afterdepolarizations in a model for human ventricular tissue, N. Vandersickel, I.V. Kazbanov, A. Nuitermans, L.D. Weise, R. Pandit, and A.V Panfilov, PLOS ONE 9(1): e84595 (2014).
- Spiral-wave dynamics in ionically realistic mathematical models for human ventricular tissue: the effects of periodic deformation, A.R. Nayak and R. Pandit, Frontiers in Physiology Vol. 5, 207 (2014); doi: 10.3389/fphys.2014.00207.
- Turbulent electrical activity at sharp-edged inexcitable obstacles in a model for human cardiac tissue, R. Majumder, R. Pandit, and A.V. Panfilov, Am. J of Physiol Heart Circ. Physiol., 307(7):H1024âĂŞH1035, (2014).
- A Comparative Study of Early Afterdepolarization-Mediated Fibrillation in Two Mathematical Models for Human Ventricular Cells, S. Zimik, N. Vandersickel, A.R. Nayak, A.V. Panfilov, and R. Pandit, PLoS ONE, 10(6):e0130632, (2015).

Publications

- Turbulent states and their transitions in mathematical models for ventricular tissue: The effects of random interstitial fibroblasts, A.R. Nayak and R. Pandit, Phys. Rev. E, 92:032720, (2015).
- A computational study of the factors influencing the pvc-triggering ability of a cluster of early afterdepolarization-capable myocytes, S. Zimik, A.R. Nayak, and R. Pandit, PLoS ONE, 10 (12):e0144979, (2015).
- Scroll-wave dynamics in the presence of ionic and conduction inhomogeneities in an anatomically realistic mathematical model for the pig heart, R. Majumder, R. Pandit, and A.V. Panfilov, PisâĂŹma v ZhETF (JETP, Russia), (2016).
- Instability of spiral and scroll waves in the presence of a gradient in the fibroblast density: the effects of fibroblastâĂŞmyocyte coupling, S. Zimik and R. Pandit, New J. Phys., 18:123014, (2016).

Publications

- The effects of fibroblasts on wave dynamics in a mathematical model for human ventricular tissue, A.R. Nayak and R. Pandit, In R.P. Mondaini, editor, Proceedings of the International Symposium on Mathematical and Computational Biology, pages 363âĂŞ 378. World Scientific, Singapore, (2016).
- Spiral-wave dynamics in a Mathematical Model of Human Ventricular Tissue with Myocytes and Purkinje fibers, A.R. Nayak, A.V. Panfilov, and R. Pandit, Phys. Rev. E, 95:022405, (2017).
- Reentry via high-frequency pacing in a mathematical model for human-ventricular cardiac tissue with a localized fibrotic region, S. Zimik and R. Pandit, Scientific Reports, 7:15350, (2017).

Outline

- Motivation
  - Spatiotemporal chaos and its control in cardiac arrhythmias.
  - Effects of inhomogeneities, fibroblasts, mechanical deformation, and Purkinje fibers.
  - Effects of fiber orientation and anatomically realistic geometry.
- Models for cardiac tissue.
- Suppressing cardiac chaos.

Outline

- Numerical simulations:
  - the effects of conduction and ionic inhomogeneities;
  - the effects of fibroblasts;
  - the effects of fiber orientation;
  - the effects of anatomically realistic geometry;
  - the effects of mechanical deformation;
  - the effects of Purkinje fibers.
  - the effects of Early afterdepolarizations (EADs).
- Conclusions.

Motivation

- Cardiac arrhythmias, like ventricular fibrillation (VF), are a major cause of death in industrialised countries.
- VF: associated with broken spiral waves of electrical activation on cardiac tissue.
- Goals:
  - Understand the dynamics of VF in the presence of tissue heterogeneities.
  - Develop low-amplitude defibrillation techniques.

The Heart

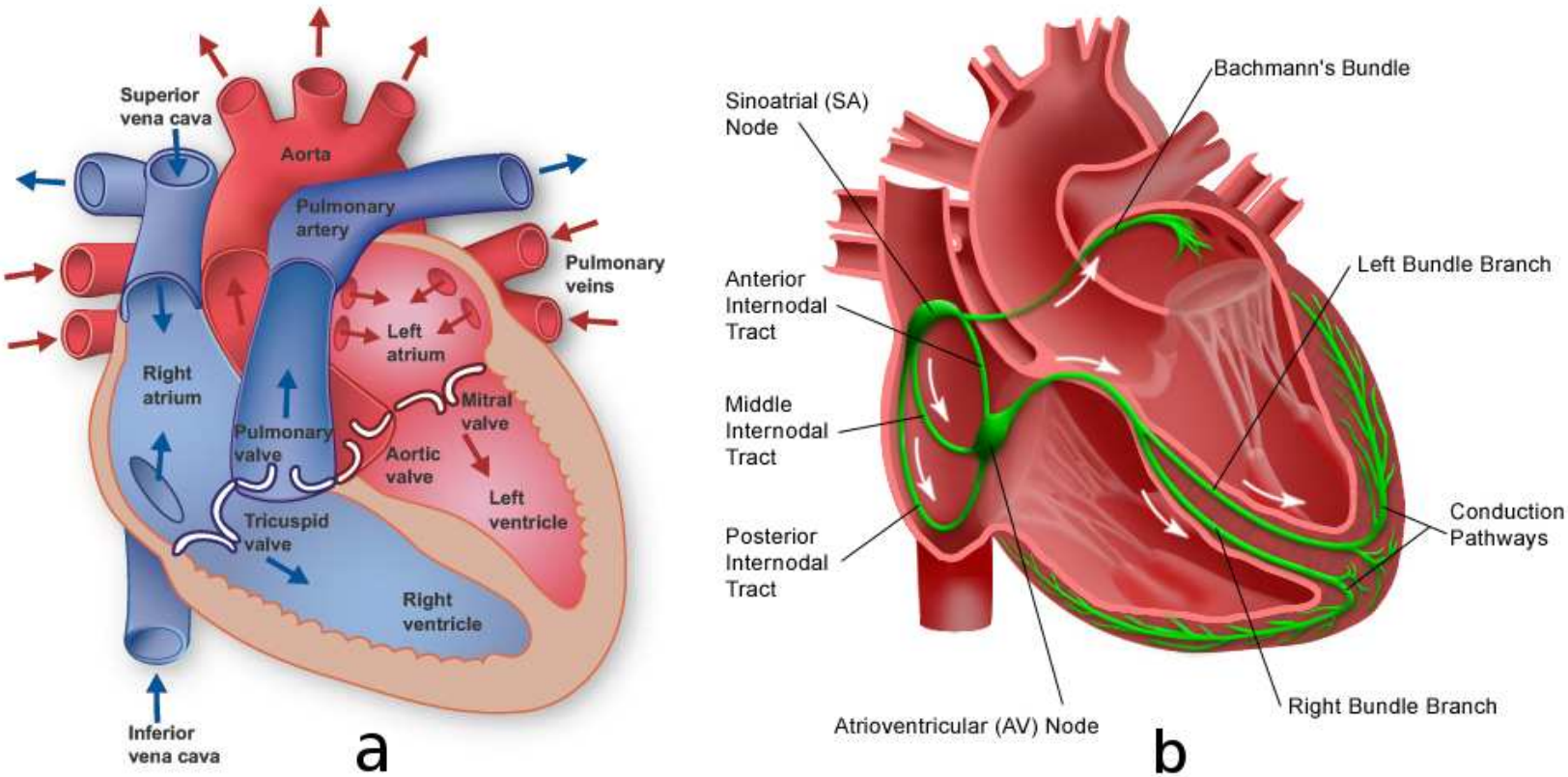

Schematic diagrams show (a) the heart anatomy and (b) its conduction systems. Images taken from: http://www.texasheartinstitute.org/HIC/Anatomy/anatomy2.cfm, http://mdmedicine.wordpress.com/2011/04/24/heart-conduction-system/.

The Heart

- One of the most efficient electro-mechanical devices.
- Rhythm: periodic contractions of atria and ventricles.
- For an average adult 72 bpm, i.e., 2.5 billion beats in an average life time.
- The rhythm is maintained by electrical activity in heart muscle.
- VT or VF destroy this rhythm.

Cardiac Arrhythmias

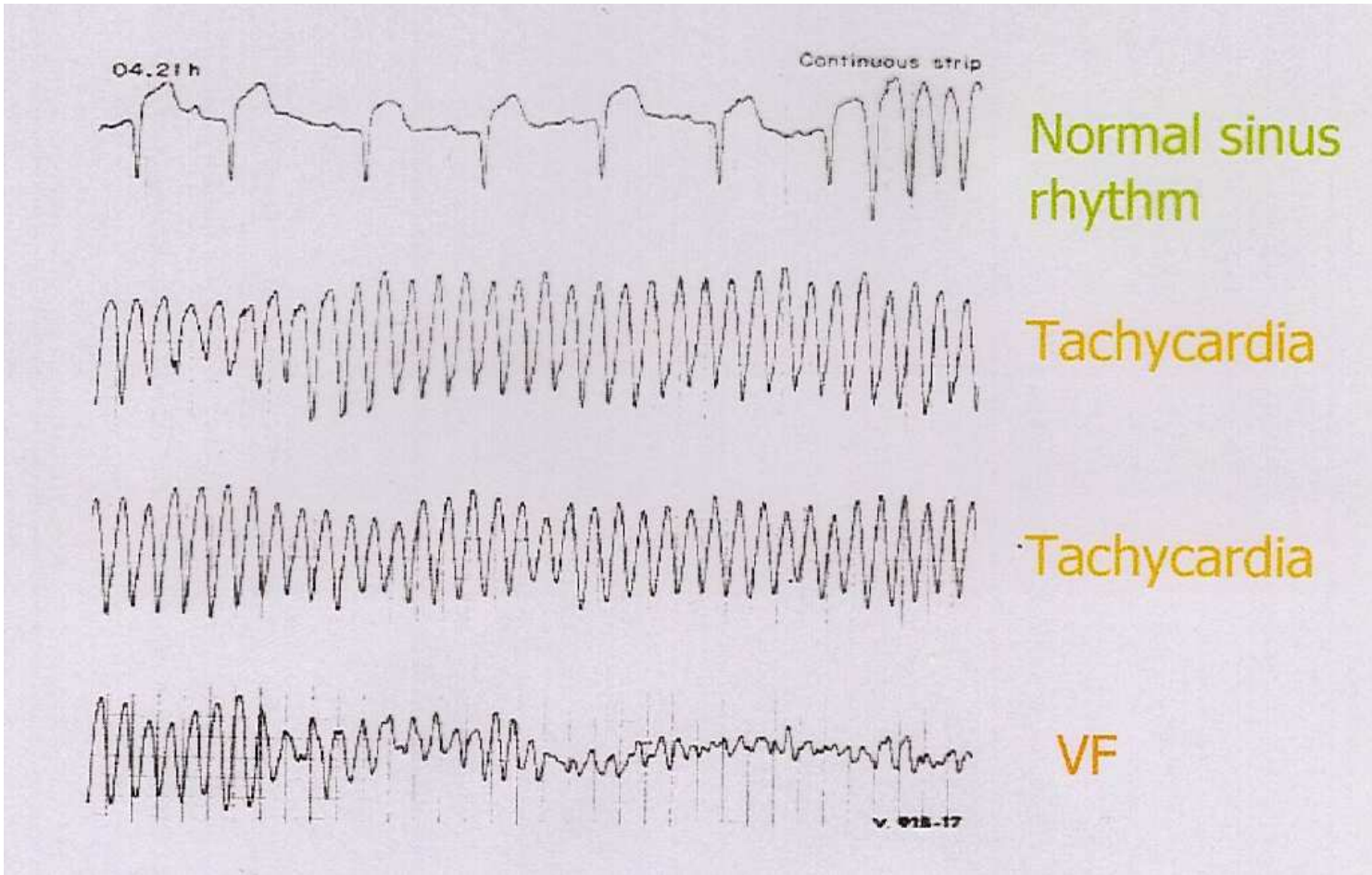

Spiral waves during VF.

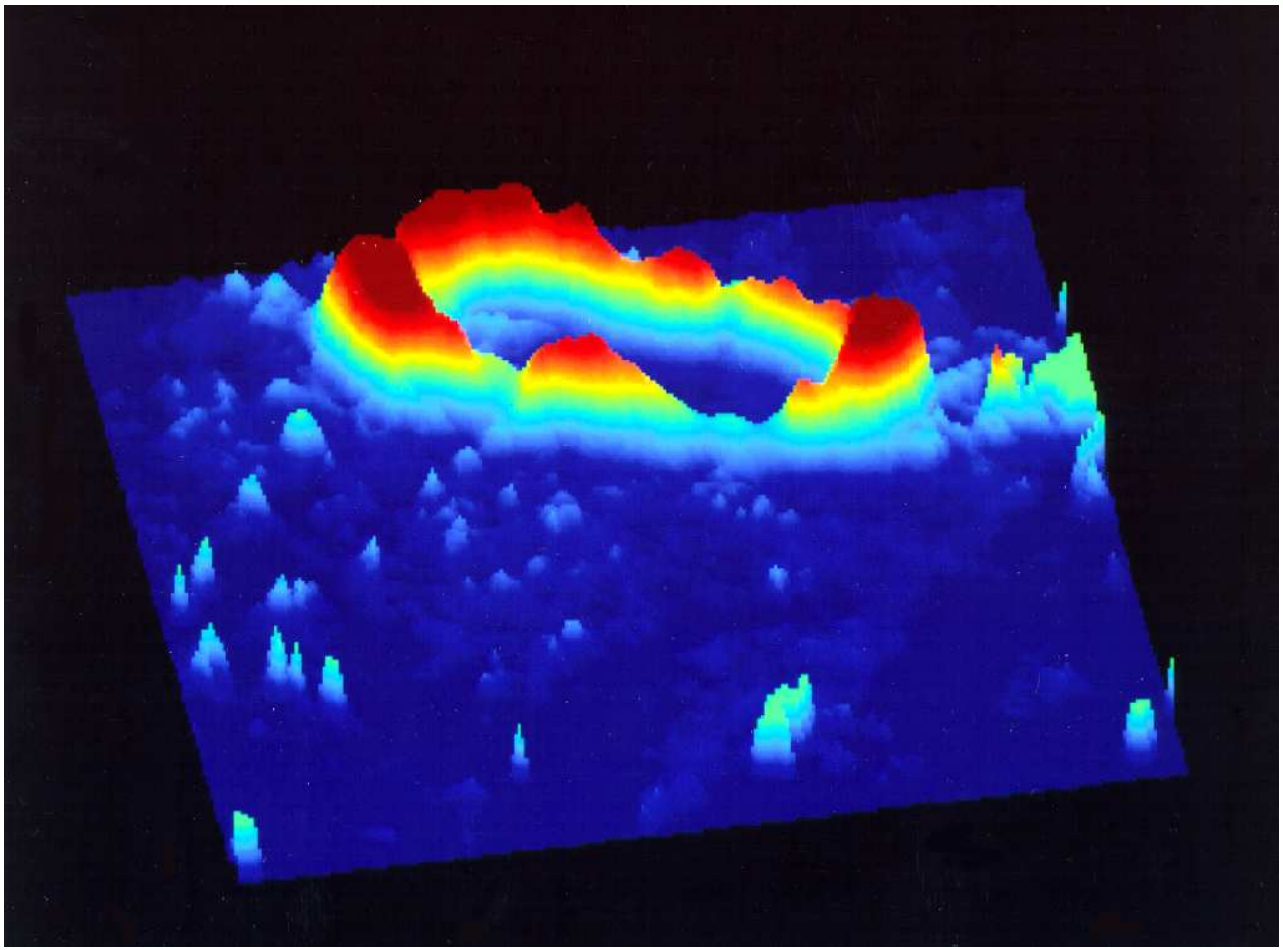

VF in a canine heart imaged via voltage sensitive dyes (from W. Ditto).

Ventricular Fibrillation

Animation

Excitability

- Excitation: electrical waves induce cardiac-muscle contractions that pump blood.
- Threshold: the membrane potential of cardiac muscle must exceed ($\simeq$ -60 mV) before the action potential is observed.
- Once excited, cardiac cells cannot be excited any more during the refractory period ($\simeq$ 200 ms).

Cardiac Action Potential

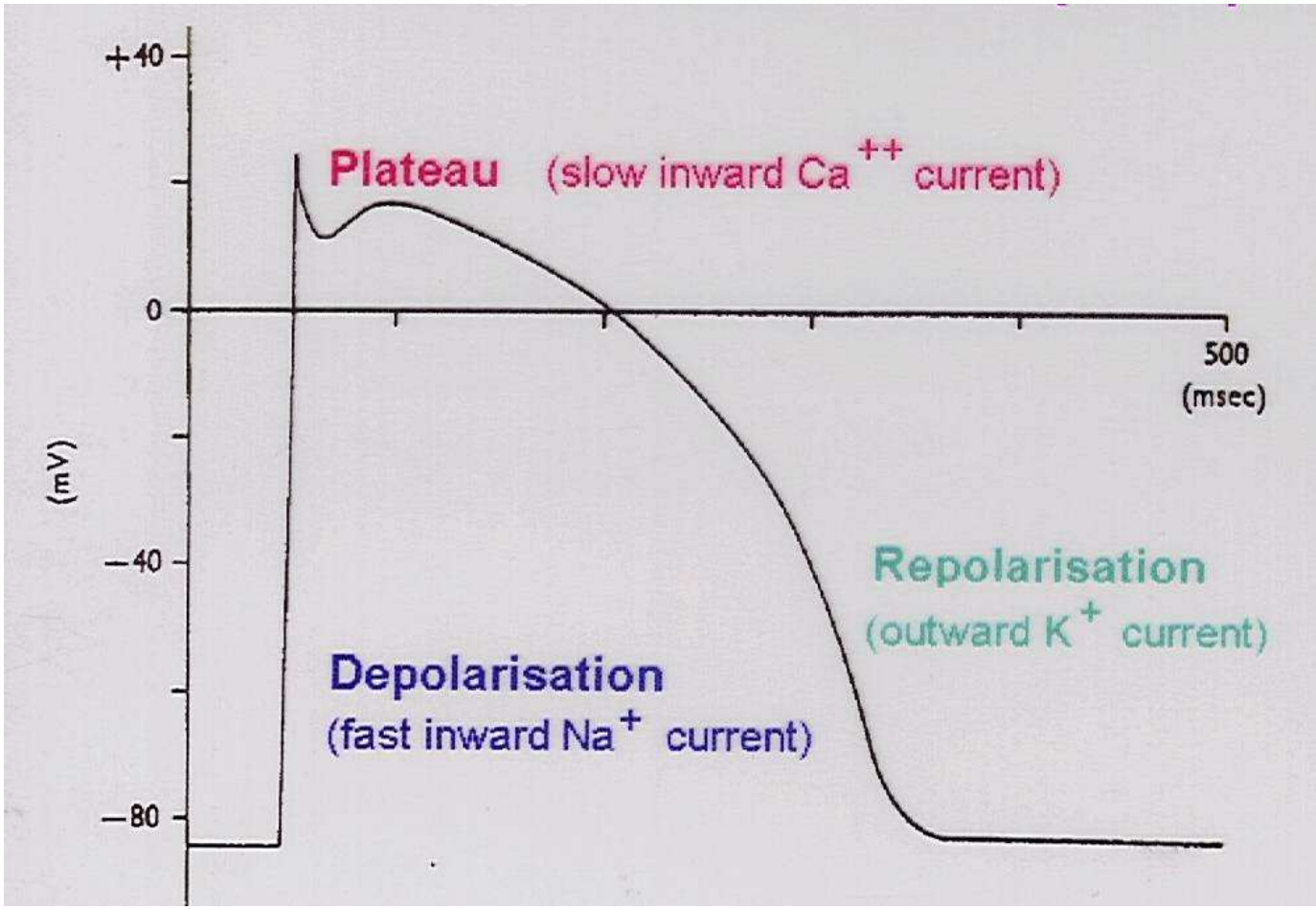

Models of Ventricular Tissue

Reaction-diffusion equation of the form

$$\frac{\partial V}{\partial t} + \frac{I}{C} = D\nabla^2 V$$

Various Models; we concentrate on:

- Panfilov Model (simplified).
- TNNP Model (human).
- TP06 Model (human).
- ORd Model (human).

The Panfilov Model

This is the simplest model that shows spiral breakup as in VF; here $e \equiv V$.

$$\begin{aligned} \partial e/\partial t &= \nabla^2 e - f(e) - g, \\ \partial g/\partial t &= \epsilon(e,g)(ke - g). \end{aligned}$$

- $f(e)$: piecewise linear;
- $\epsilon(e,g)$: information about refractory periods.

Panfilov model

$$
\begin{aligned}
f(e) &= C_1 e, e < e_1, \\
f(e) &= C_2 e + a, e_1 \leq e \leq e_2, \\
f(e) &= C_3 (e-1), e > e_2; \\
\epsilon(e,g) &= \epsilon_1, e < e_2, \\
\epsilon(e,g) &= \epsilon_2, e > e_2, \\
\epsilon(e,g) &= \epsilon_3, e < e_1, g < g_1.
\end{aligned}
$$

$e_1 = 0.0026$, $e_2 = 0.837$, $C_1 = 20$, $C_2 = 3$, $C_3 = 15$, $a = 0.06$, $\epsilon_1 = 1.75$, $\epsilon_2 = 1.0$, $\epsilon_3 = 0.3$, $g_1 = 1.8$, $k = 3$

Numerical Scheme

- Forward-Euler in time and finite- difference in space.
- Space step δx=0.5 dimensionless units.
- Time step δt=0.022 dimensionless units.
- Dimensioned time T is 5ms times dimensionless time.
- One spatial unit is 1mm. (Ref: A. V. Panfilov and P. Hogeweg, *Phys. Lett. A* **176**, 295 (1993).)

Spiral Turbulence (Panfilov Model)

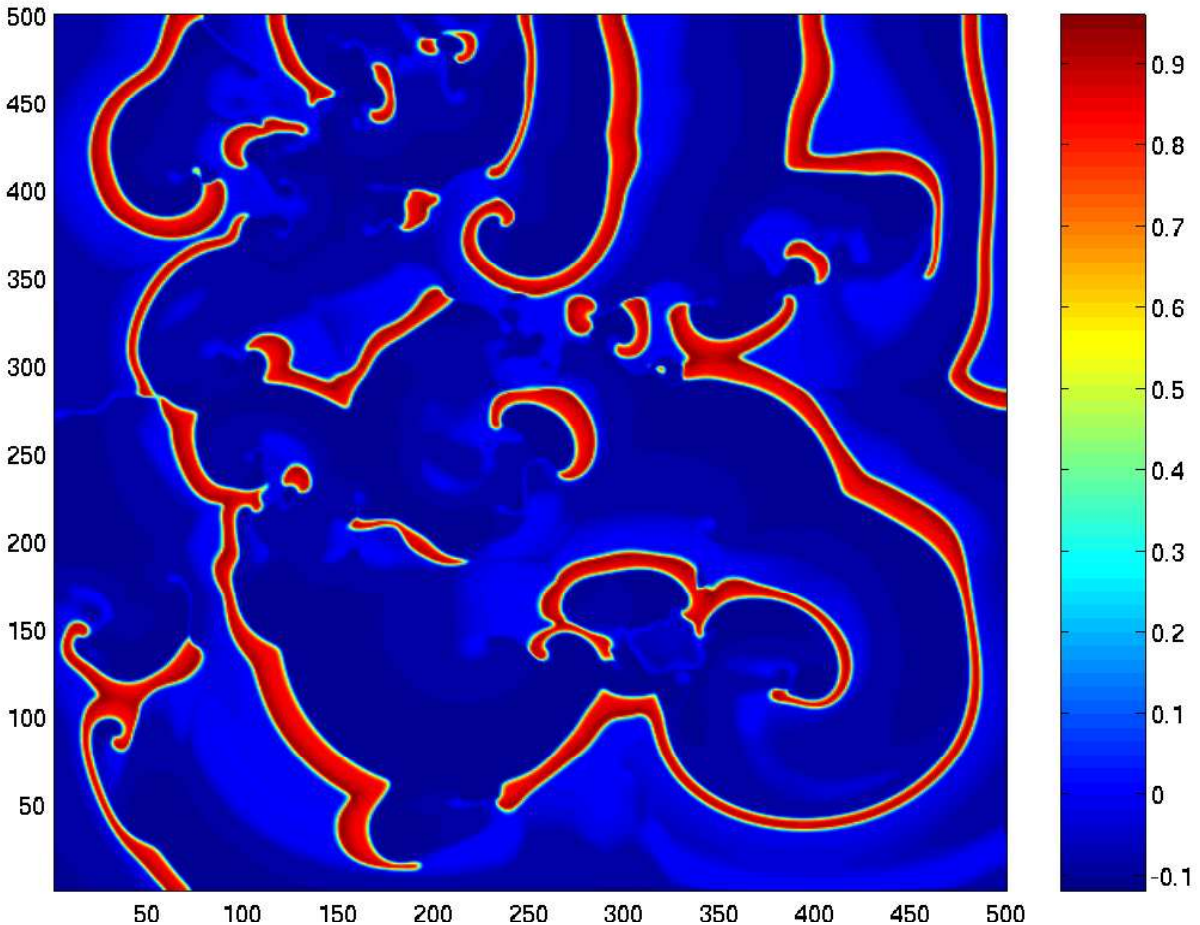

Animation

The TNNP Model

- The TNNP model is based on fairly recent experimental data on human ventricular cells.
- Biologically realistic; incorporates details of ionic currents, ion channels, ion pumps, and ion exchangers.
- It uses 12 ionic currents, 12 gating variables, intracellular Na^+ and K^+ concentrations, and Ca^{2+} concentrations in the cytoplasm and sarcoplasmic reticulum (SR).

The TNNP Model

- The reaction-diffusion equation is:

$$\frac{\partial V}{\partial t} + \frac{I_{TNNP}}{C_m} = D\nabla^2 V \qquad (1)$$

$C_m = 2\mu$F/cm^2 is the membrane capacitance, $D(cm^2/ms)$ is the diffusion coefficient and I_{TNNP} (pA) is the instantaneous total ionic current through the cell:

$$\begin{aligned} I_{TNNP} &= I_{Na} + I_{CaL} + I_{to} + I_{Ks} + I_{Kr} + I_{K1} \\ &\quad + I_{NaCa} + I_{NaK} + I_{pCa} + I_{pK} + I_{bNa} + I_{bCa}. \end{aligned}$$

Currents

- Inward currents (Na and Ca) cause depolarization.
- Outward currents (K) cause repolarization.

Currents

- This flow of ions through channels in the membrane depends on concentration gradients.
- The Nernst potential at which the chemical and electrical gradients are equal and opposite is

$$E_{ion} = \frac{RT}{nF} \ln \frac{[ion]_o}{[ion]_i}; \tag{2}$$

R : gas constant; T : temperature; n : valence of the ion; F : Faraday's constant; $[ion]_o$ and $[ion]_i$: extra- and intra-cellular ionic concentrations.

Currents

The amplitude of an ionic current depends on the conductance of the membrane and the driving force:

$$I_{ion} = \bar{G_{ion}}(V_m - E_{ion}) \tag{3}$$

Conductance $\bar{G_{ion}}$: product of the maximal conductance of all ion channels in the cell (G_{ion}) and the probability ϵ of a channel being in the open state:

$$I_{ion} = G_{ion}\epsilon(V_m - E_{ion}) \tag{4}$$

Gating Variables

- The gating variables (represented by ϵ) are the probabilities of the channels being in the open state. They obey ODEs of the form:

$$\frac{d\epsilon}{dt} = \alpha_\epsilon(1-\epsilon) - \beta_\epsilon\epsilon;$$

α_ϵ and β_ϵ : are the rates at which gates open and close.

Gating Variables

Steady-state: $d\epsilon/dt = 0$ yields

$$\epsilon_\infty = \frac{\alpha_\epsilon}{(\alpha_\epsilon + \beta_\epsilon);} \tag{5}$$

$$\epsilon = \epsilon_\infty - (\epsilon_\infty - \epsilon_0)\exp(-t/\tau); \tag{6}$$

$$\tau = 1/(\alpha_\epsilon + \beta_\epsilon). \tag{7}$$

Rate Constants

By measuring the voltage dependences of ϵ and τ and by using the above equations we can obtain α_ϵ and β_ϵ for each value of the membrane potential.

Numerical Method

- Forward Euler in time and finite difference in space (5-point stencil for the Laplacian).
- δt=0.02ms, δx=0.0225 cm.
- The resting-state value of V is -86.2 mV. All gating variables (ϵ) are initialised to their steady-state values, i.e., ϵ_∞.
- We use Neumann (no-flux) boundary conditions on a square simulation domain containing 600×600 grid points.

MPI Simulation Technique

- MPI code: we divide our simulation domain into n columns.
- If our square simulation domain contains $N \times N$ grid points, then each processor carries out computations for $N \times (N/n)$ grid points.
- At the interfaces of processor boundaries we use two extra temporal grid lines which can send and receive the data from left- and right-neighbour processors.
- We have developed an MPI code for the TNNP model; this can be run in both Windows and Linux clusters.

Simulation Technique

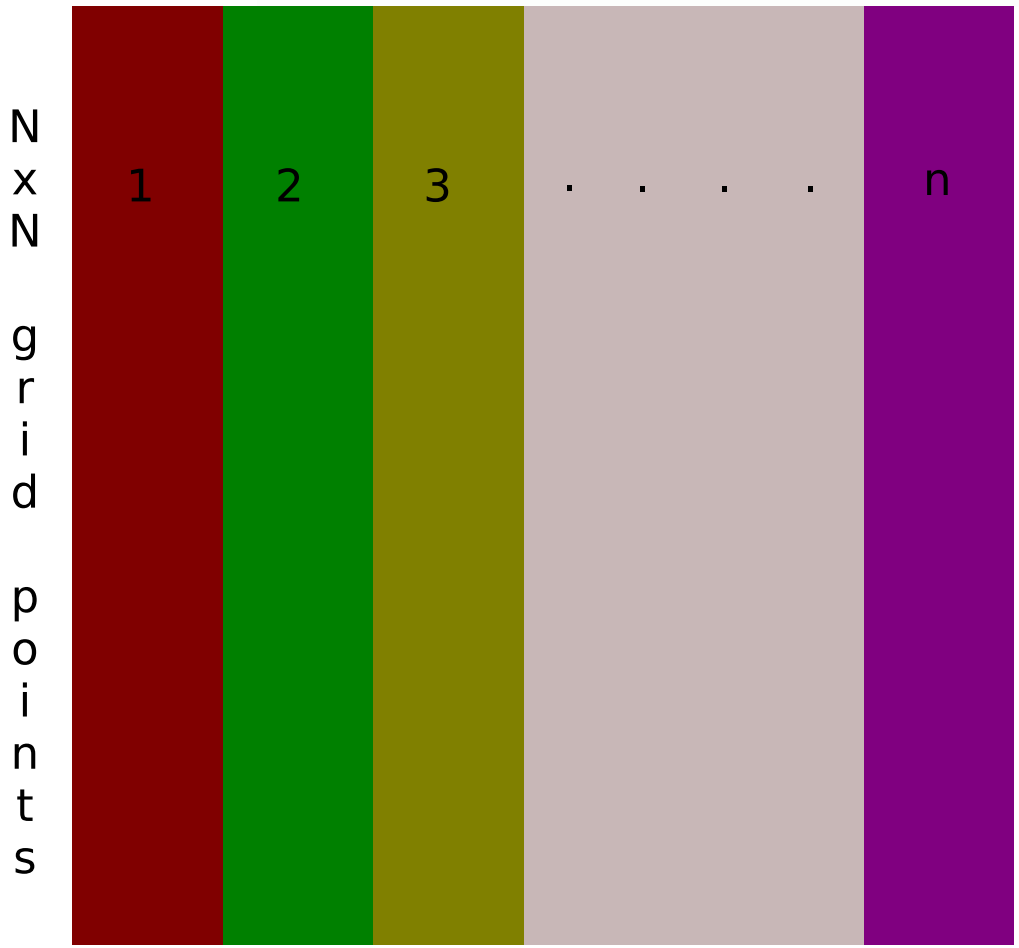

Schematic diagram of our MPI simulation, here n represents to the number of processor.

Performances of the clusters

- We have tested our MPI code on various high-performance computing (HPC) platforms.
- The computation time decreases roughly linearly as we increase the number of processors.

HPC Performance

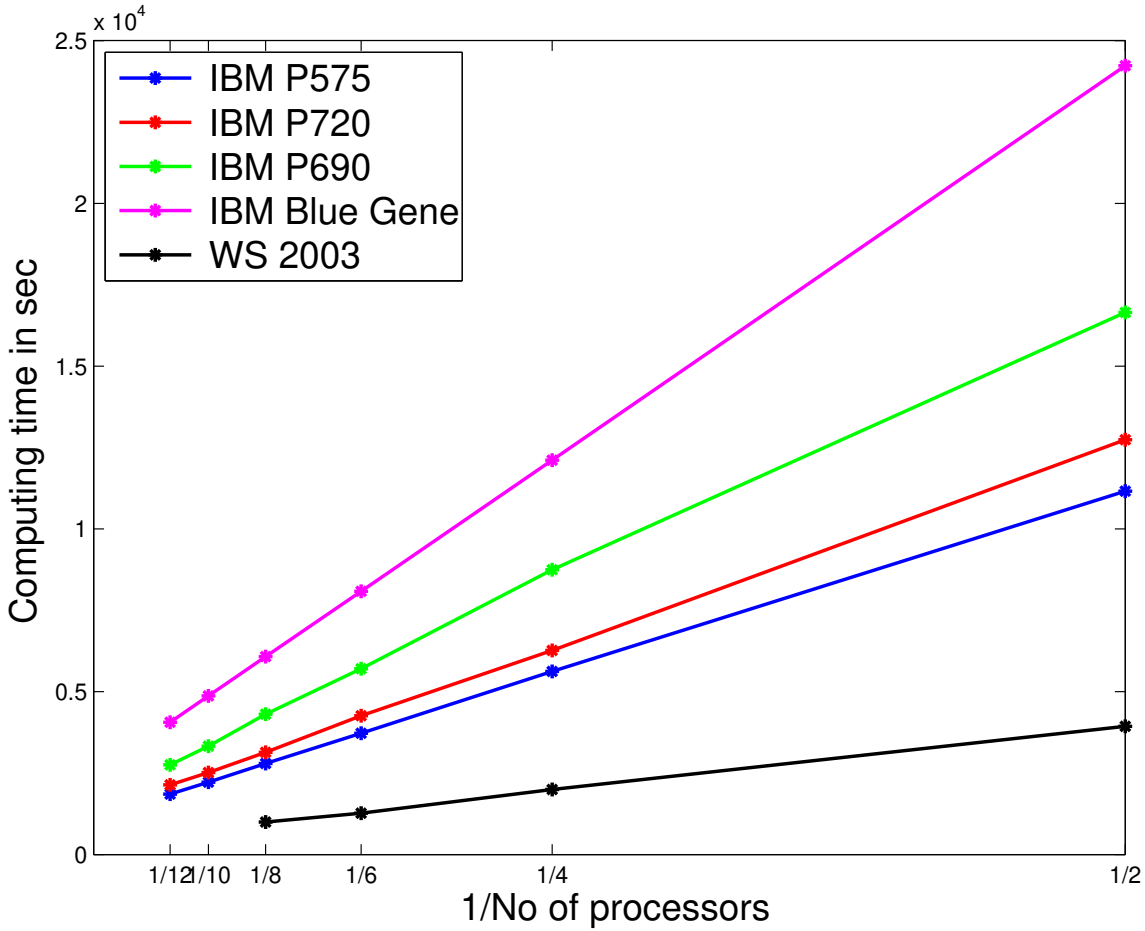

A plot of computing time versus the inverse of the number of processors for our MPI code for the TNNP model (600×600 domain).

Spiral-wave Initiation

- A stimulus of strength 150 μA/cm^2 is applied at the left boundary for 3 ms; this initiates a plane wave.
- A second stimulus of strength 450 μA/cm^2 is applied, after 560 ms and just behind the refractory tail of S1, along $x = 360$, $1 \leq y \leq 550$, for 3 ms.
- This produces a second wave front with a free end around which the wave curls to produce a spiral.

Rotating-spiral (RS) State

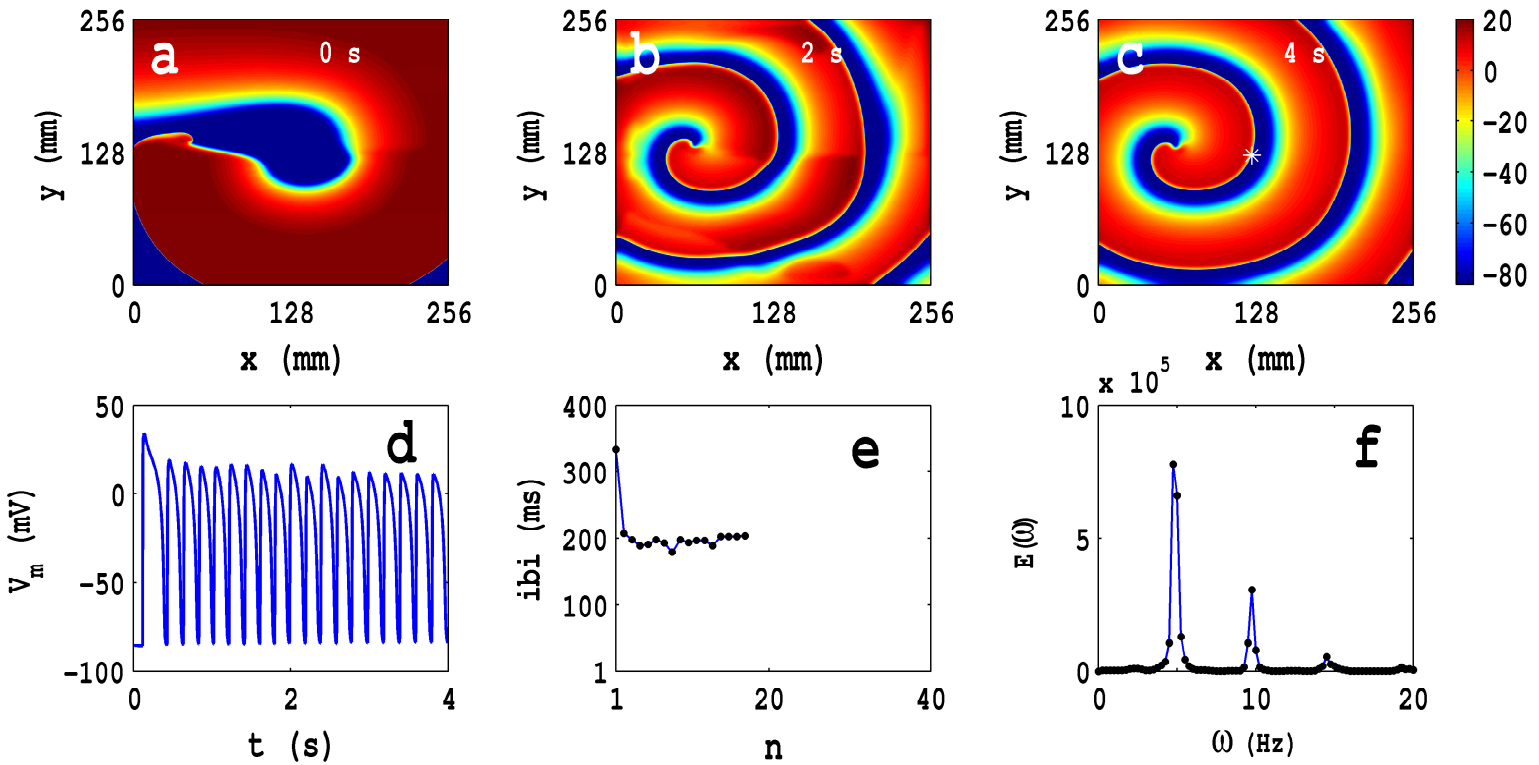

The TP06 model with the P1 parameter set shows an RS state in homogeneous domain.

Single-meandering-spiral-turbulence (SMST) State

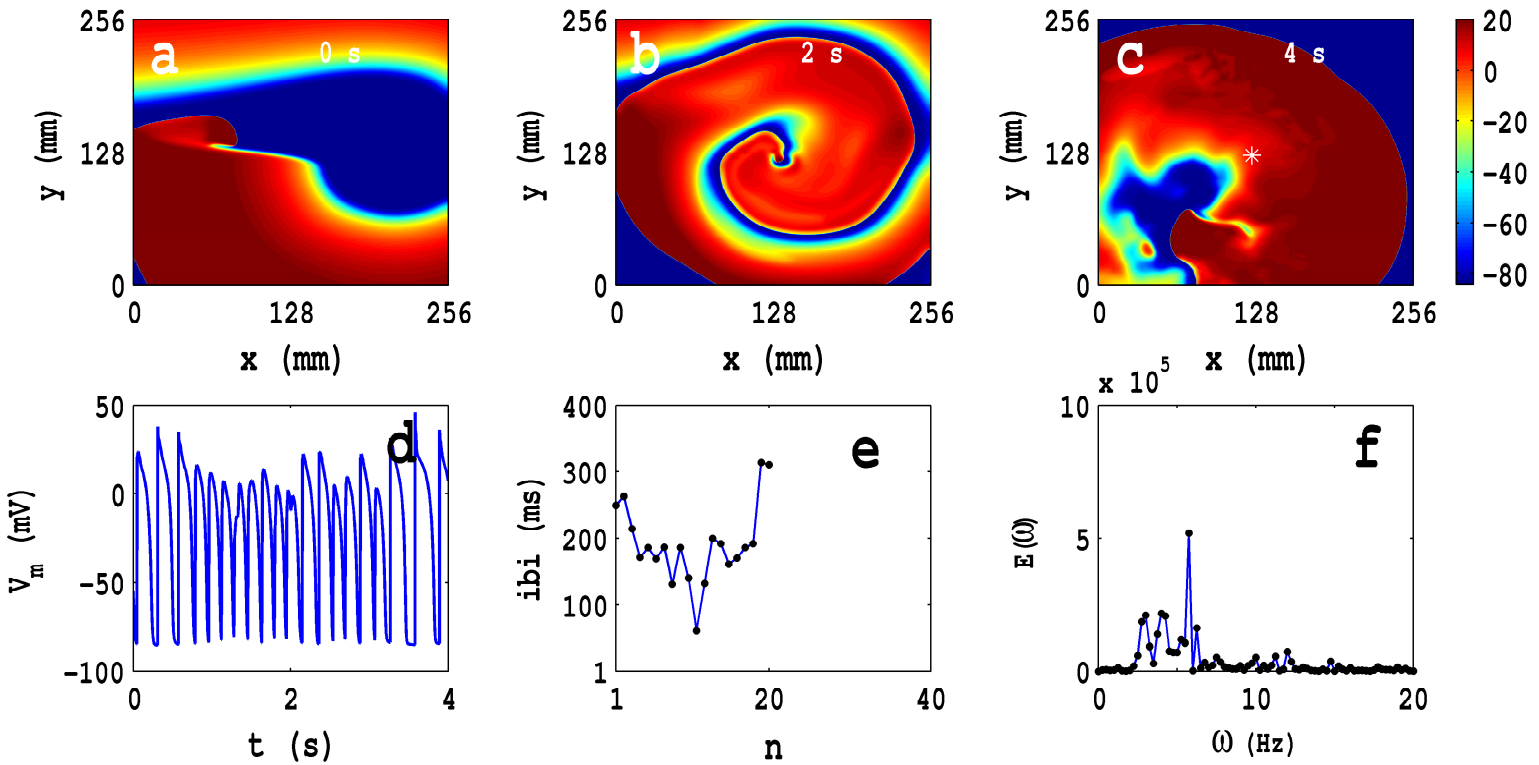

The TP06 model with the P2 parameter set shows an SMST state in homogeneous domain.

Multiple-spiral-turbulence (MST) State

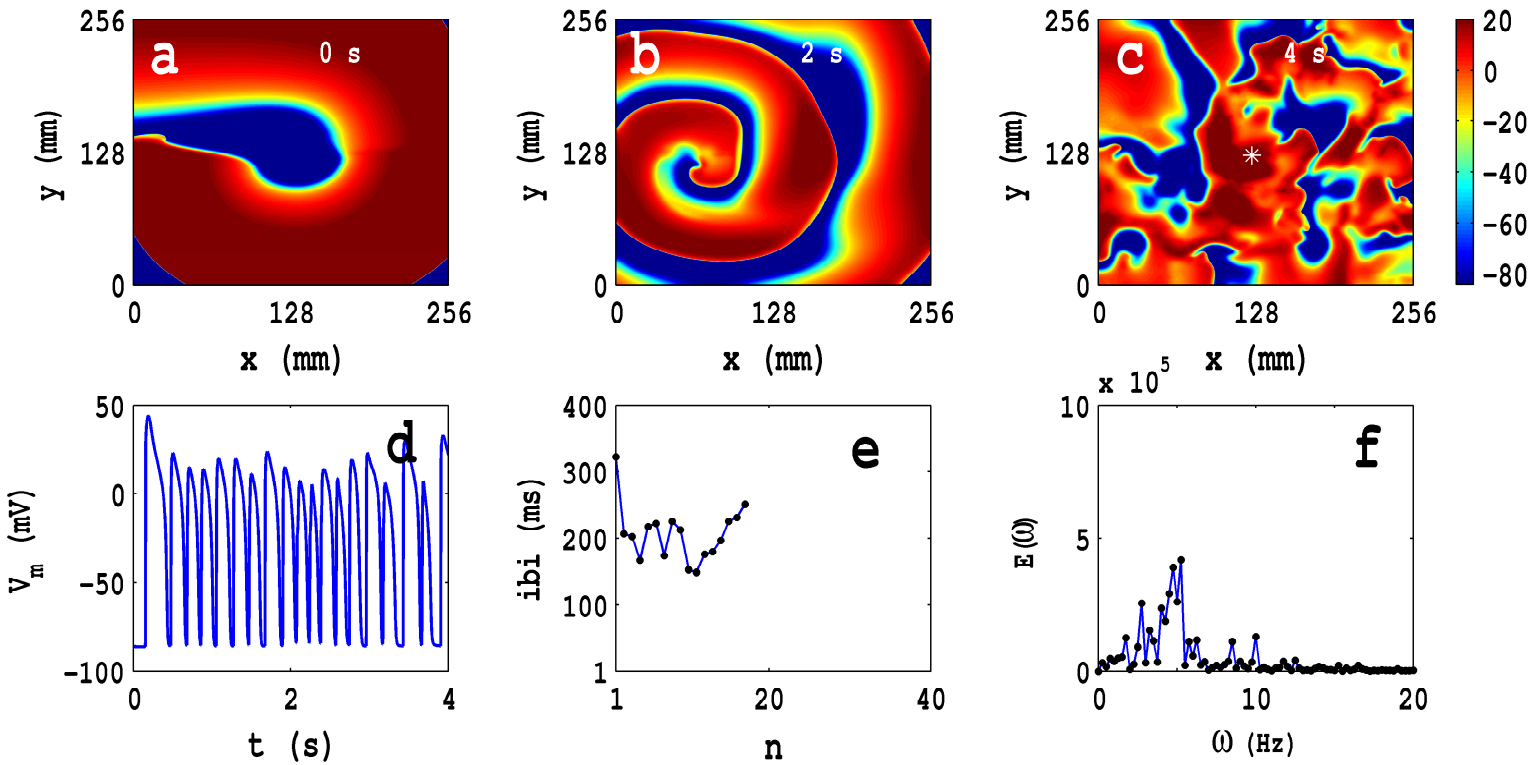

The TP06 model with the P3 parameter set shows an MST state in homogeneous domain.

Animation

Defibrillation

- Pharmaceutical means: Administer medication ...
- Electrical means:
  - Electrical defibrillation: Two paddles are placed on the chest and a large electric shock ($\sim$ 5 kV) applied across them.
  - Internal defibrillation: Administer electrical shocks (~ 600 V) through an implantable electrical defibrillator which also detects the onset of VF.

Defibrillation

Example of an implantable cardiac defibrillator (ICD)

Vol 54 cc
Mass 97 gm
Thickness 16mm
Longevity 9 yrs
BOL Voltage 6.4 V
ERI 4.91 V
BOL Charge time 6.0 sec

Defibrillation

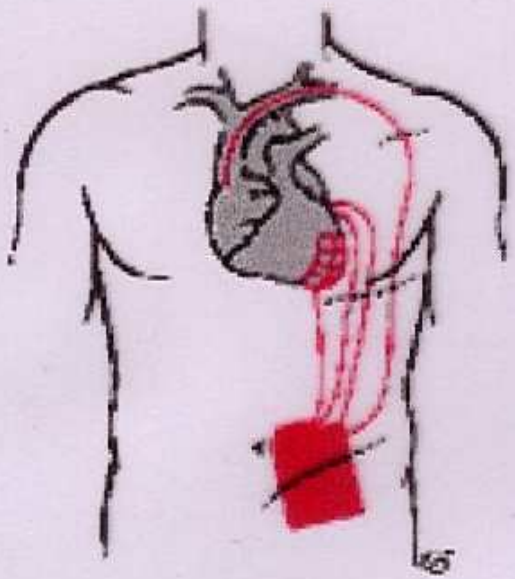

An internal defibrillating system consists of a pulse generator and electrical leads. Endocardial leads are inserted into the venous system, usually via the subclavian or cephalic vein and advanced to the right ventricle and/or atrium. The pulse generator is placed subcutaneously or submuscularly and connected to the leads.

Control in 2-D Models

- The models have non-conducting boundaries (*no-flux* or *Neumann* boundary conditions): ventricles are electrically insulated from atria.
  Observations:
- Non-conducting boundaries absorb spiral defects.
- Spirals do not last for appreciable periods in small systems.

Operating Principles

- Divide the system ($L \times L$) into K^2 smaller blocks.
- Isolate the blocks (size L/K) by stimulating the system along the block boundaries - making them refractory.

Operating Principles

- Each block is too small to sustain spiral activity - spirals absorbed by block boundaries.
- After the system is driven to the quiescent state, controlling stimulation is withdrawn- block boundaries recover from refractory state.

Without Control

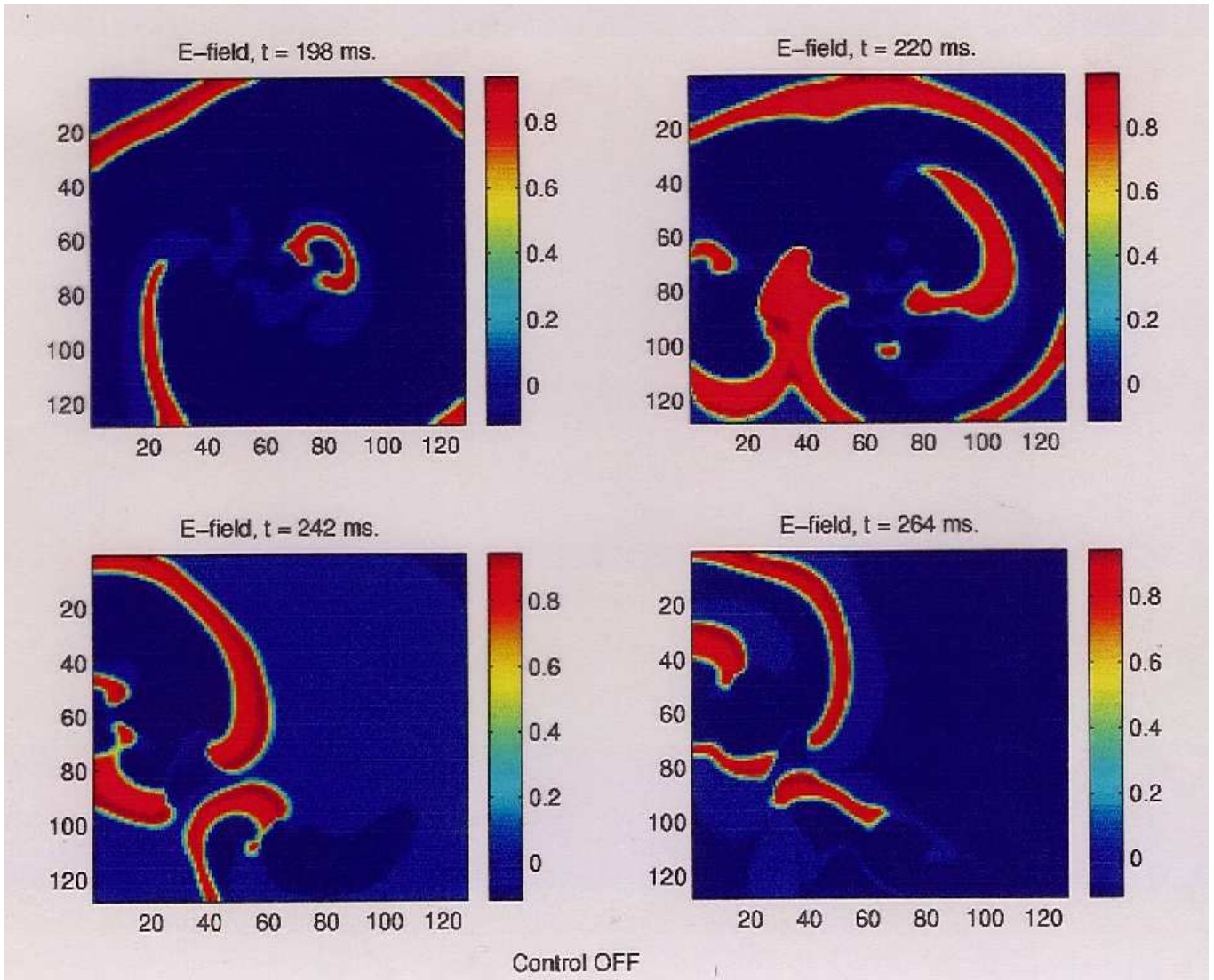

Control ON

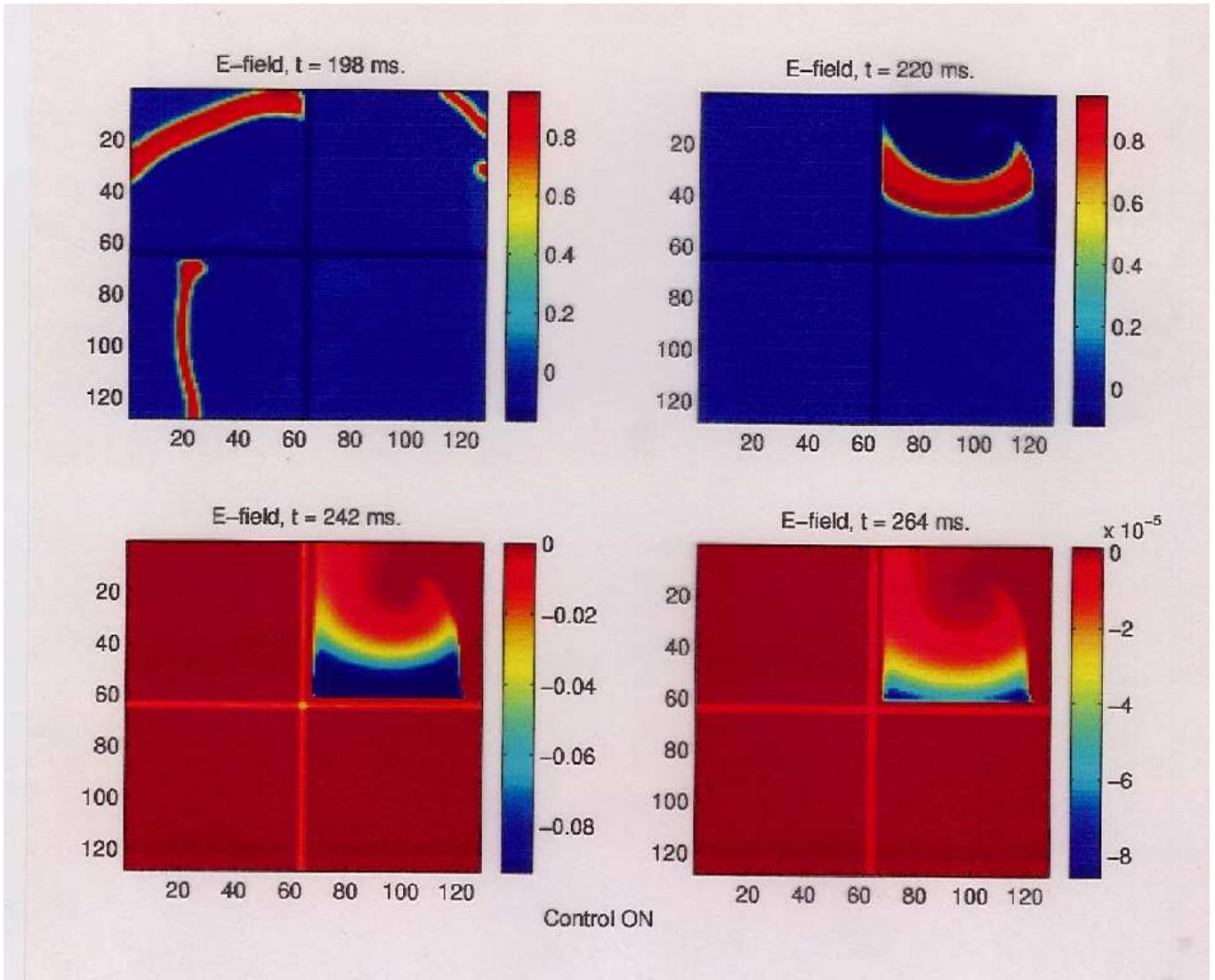

Animation

Control Parameters in 2-D

- Panfilov Model
  L = 256
  Pulse amplitude $\simeq$ 57.3 mV/ms.
  Kept on for τ = 41.2 ms.
  This implies a defibrillation current density of 57 μ A/cm^2.

Control in 2-D Panfilov

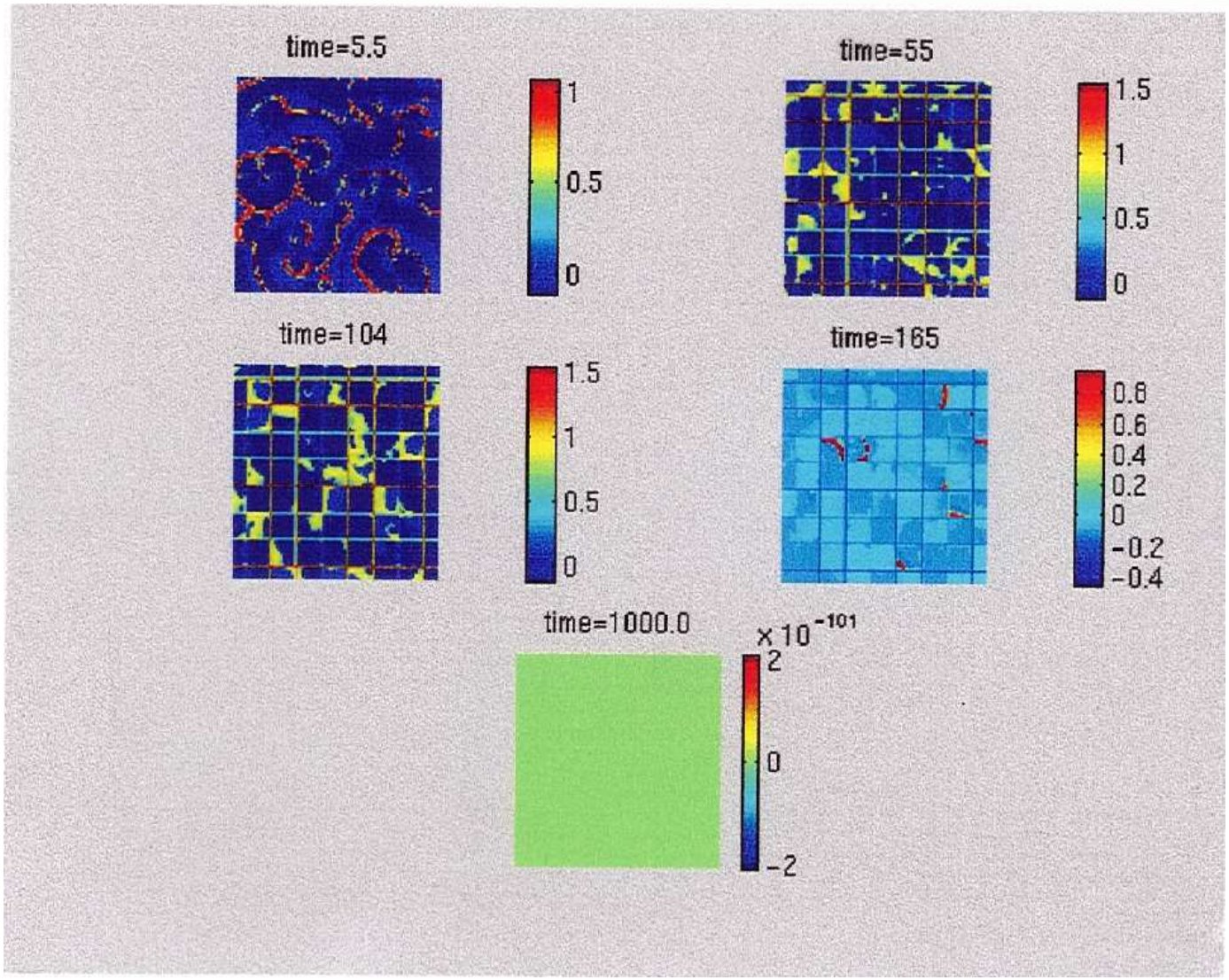

Control in TP06 Model

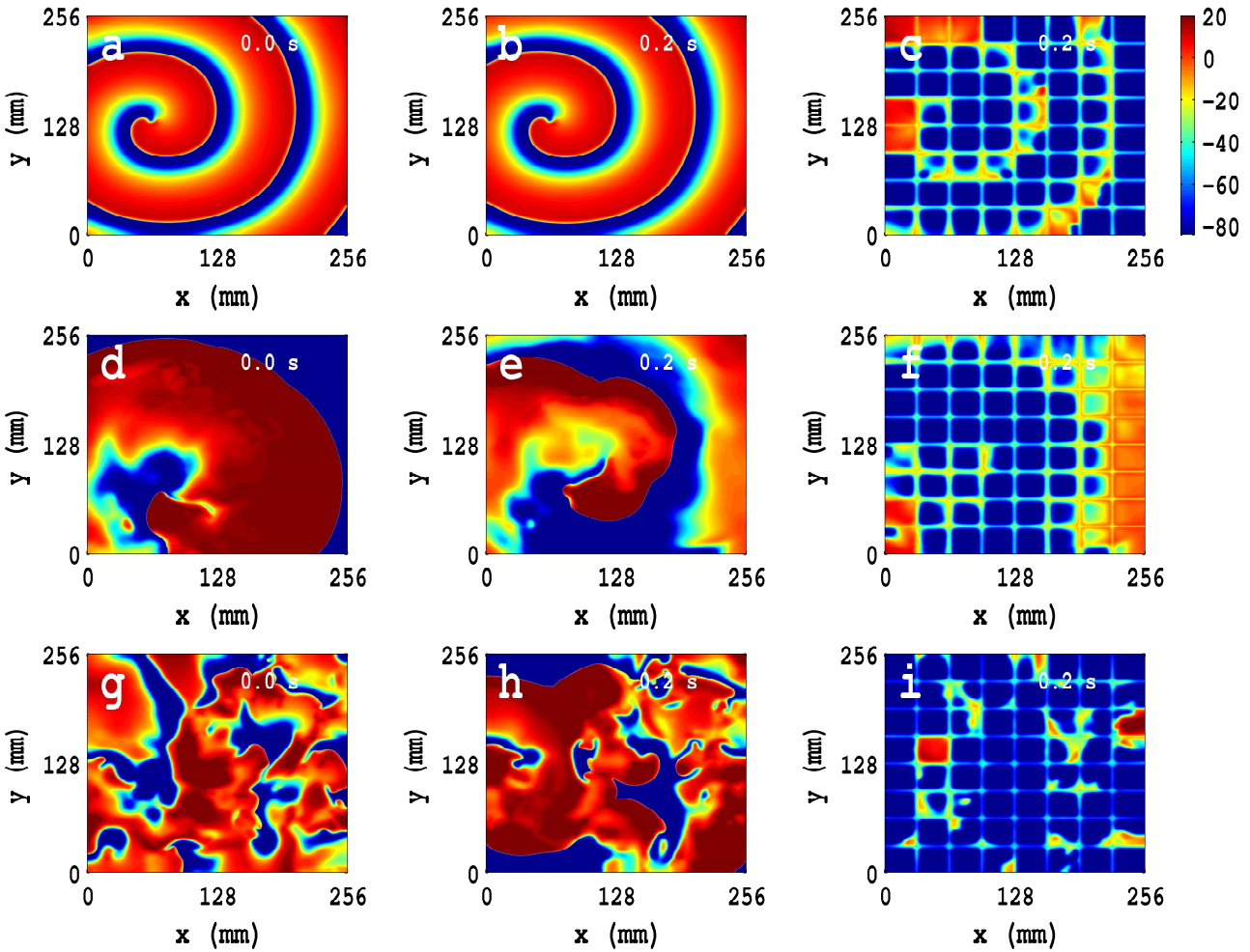

Animation

Spiral-wave control in the TP06 model for the homogeneous domain by low-amplitude control pulses.

Panfilov Model : Control in 3-D

Control algorithm as in 2-D with the following modifications:

- Control mesh only on free face of a 3-D domain ($L \times L \times L_z$).
- With L = 256 control obtained for L_z.

Panfilov Model : Control in 3-D

For L_Z >4 pulsed control is necessary:

- activate control mesh after τ ms;
- keep it on for τ_{ON} ms;
- turn it off for τ_{OFF} ms;
- keep it on for τ_{ON} ms;
- repeat n times.
  We find τ_{ON}=0.11 ms, τ_{OFF}=22 ms and $n = 30$ suffices. τ_{OFF} is comparable to the duration of one action potential.

3D Control

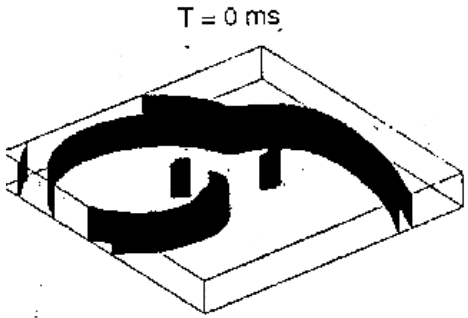

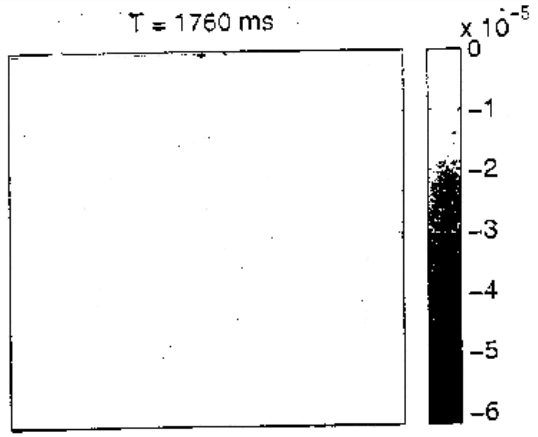

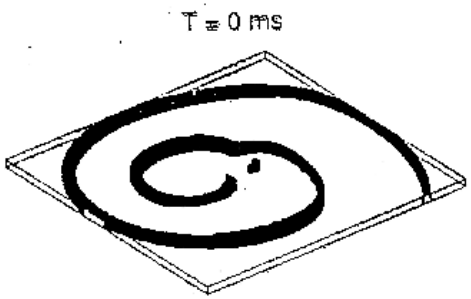

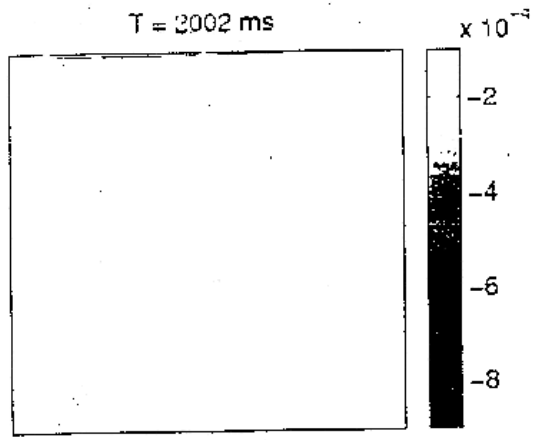

Patent

Patent granted: Government of India PATENT No. 199042 (date of grant 1/03/2006) - for an Improved System for Ventricular Defibrillation. This is owned by the Indian Institute of Science; it is based on work done in our group with my students and postdoctoral fellows, namely, Ashwin Pande, Sitabhra Sinha, and Avishek Sen.

Nonconducting Obstacles

Such inhomogeneities and obstacles, present in cardiac tissue, can yield the following:

- Spiral breakup, i.e., VF.
- Partial suppression, i.e., VF $\rightarrow$ VT transition.
- Complete suppression of VF.

Nonconducting Obstacles

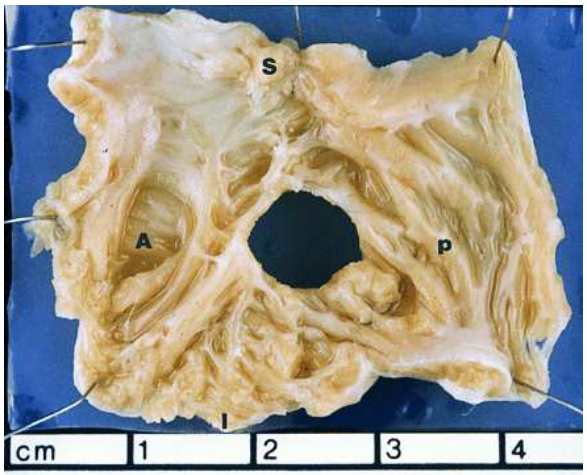

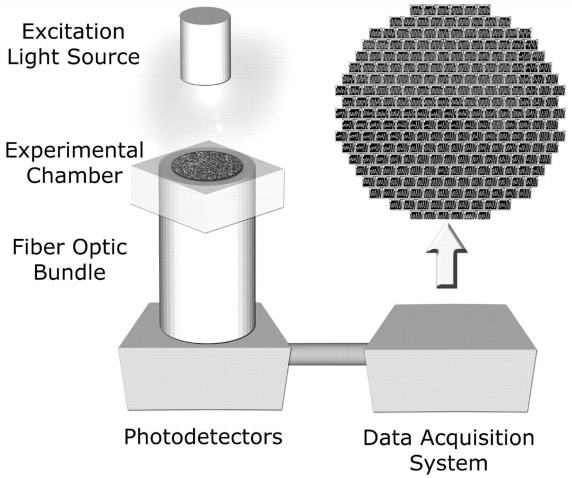

Spiral Wave Attachment to Millimeter-Sized Obstacles

Zhan Yang Lim, MS; Barun Maskara, MS; Felipe Aguel, PhD;
Roland Emokpae, Jr, BS; Leslie Tung, PhD

Background—Functional reentry in the heart takes the form of spiral waves. Drifting spiral waves can become pinned to anatomic obstacles and thus attain stability and persistence. Lidocaine is an antiarrhythmic agent commonly used to treat ventricular tachycardia clinically. We examined the ability of small obstacles to anchor spiral waves and the effect of lidocaine on their attachment.

Nonconducting Obstacles

In our models we have introduced nonconducting inhomogeneities and we find all the three types of behaviours mentioned above:

- Sometimes the inhomogeneity causes spiral breakup (red).
- Sometimes it suppresses VF partially and converts it into VT (blue).
- It can even suppress VF completely (green).

Obstacle: Panfilov Model, ST

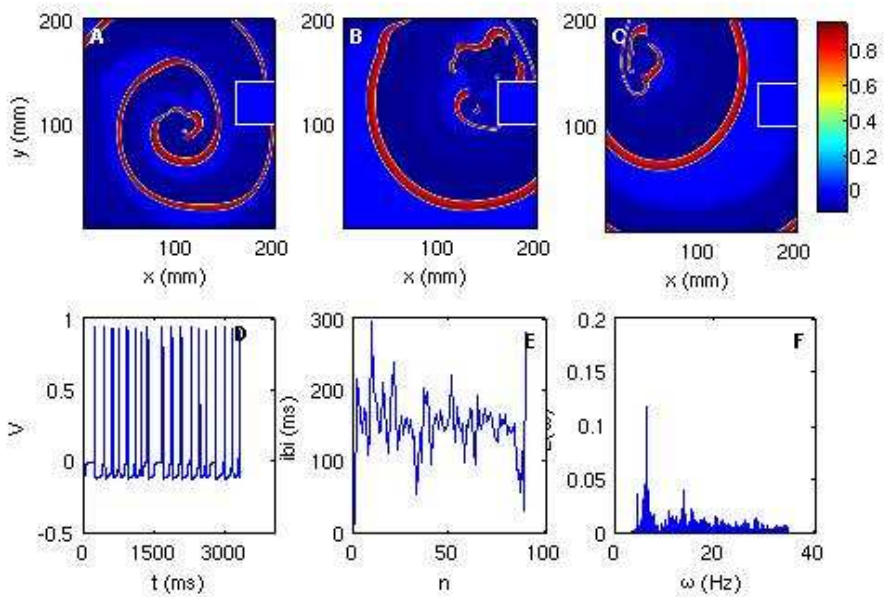

When an obstacle of side 40 mm is placed at (x =150 mm, y=100 mm) the spiral breaks up. A, B and C show snapshots at time 1100 ms, 1650 ms and 2750 ms, respectively. The local time series, interbeat interval IBI,and power spectrum of the transmembrane potential e(x,y,t) are shown in D, E, and F, respectively.

Obstacle: Panfilov Model, RS

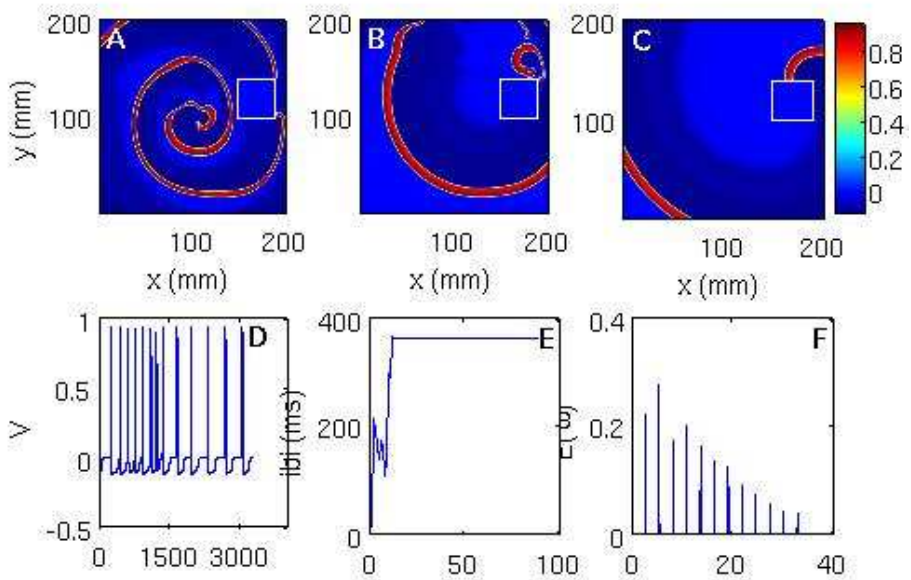

When an obstacle of side 40 mm is placed at (x =150 mm, y=100 mm) the spiral gets attached to it. A, B and C show snapshots at time 1100 ms, 1650 ms and 2750 ms, respectively. The wave gets attached to the obstacle.

Obstacle: Panfilov Model, NS

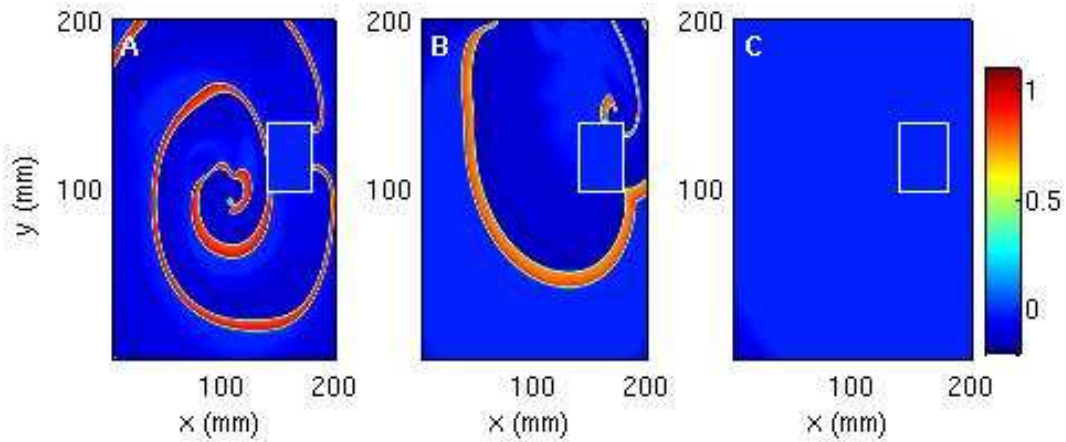

Spiral wave moves away when a square obstacle of side 40 mm is placed in the medium such that its lower-left corner is at (x =140 mm, y=100 mm) the the spiral moves away from the medium. A, B and C show snapshots at time 1100 ms, 1650 ms and 2750 ms, respectively.

Stability Diagram

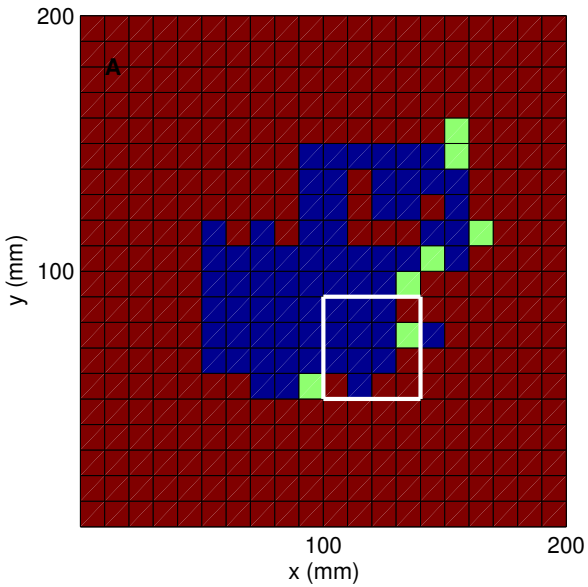

The colour of each small square indicates the final state of the system: red indicates spiral turbulence, blue a single anchored spiral, and green a quiescent state with no spirals, when the position of the lower-left hand corner of the obstacle coincides with that of the small square.

Stability Diagram: TNNP Model

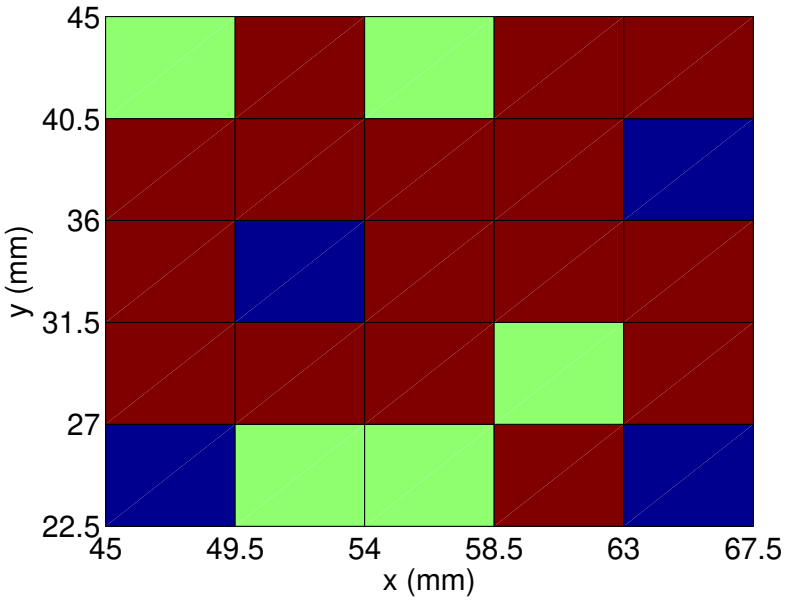

The colour of each small square indicates the final state of the system: red indicates spiral turbulence, blue a single anchored spiral, and green a quiescent state with no spirals, when the position of the lower-left hand corner of the obstacle coincides with that of the small square.

Obstacle: 3D TNNP model

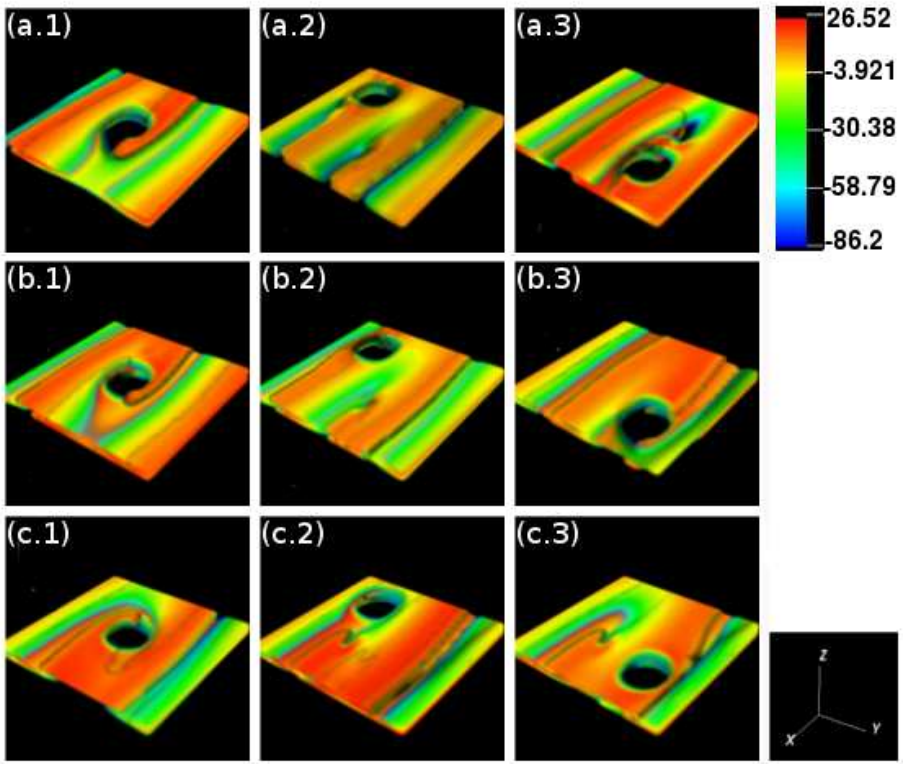

A comparison of the sensitive dependencies of scroll-wave dynamics in a slab of simulated human cardiac tissue under the coupled effect of FR (top to bottom) and the presence of cylindrical conduction-type inhomogeneities, for 3 different positions of the obstacle (left to right).

Anatomically realistic model: Panfilov model

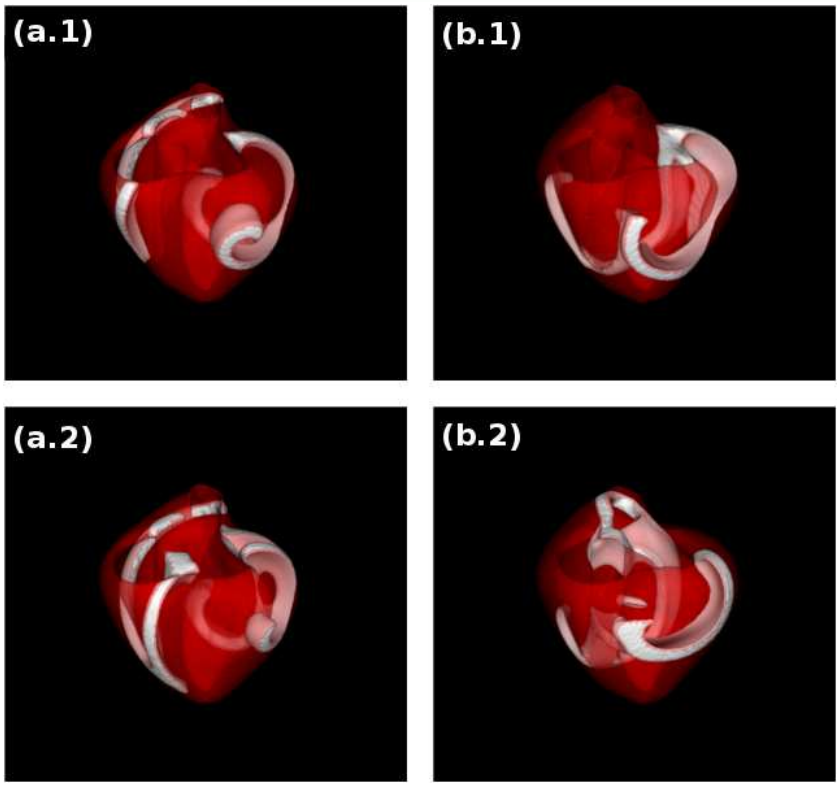

Spatiotemporal evolution of a scroll wave in an anatomically realistic domain (ventricles of a porcine heart) for the Panfilov model: (a.1) and (a.2) scroll waves at t= 0.99 s and 3.8 s and ϵ_1= 0.05; (b.1) and (b.2) broken scroll waves at t= 0.99 s and 3.8 s and ϵ_1= 0.01.

Anatomically realistic model: Panfilov model

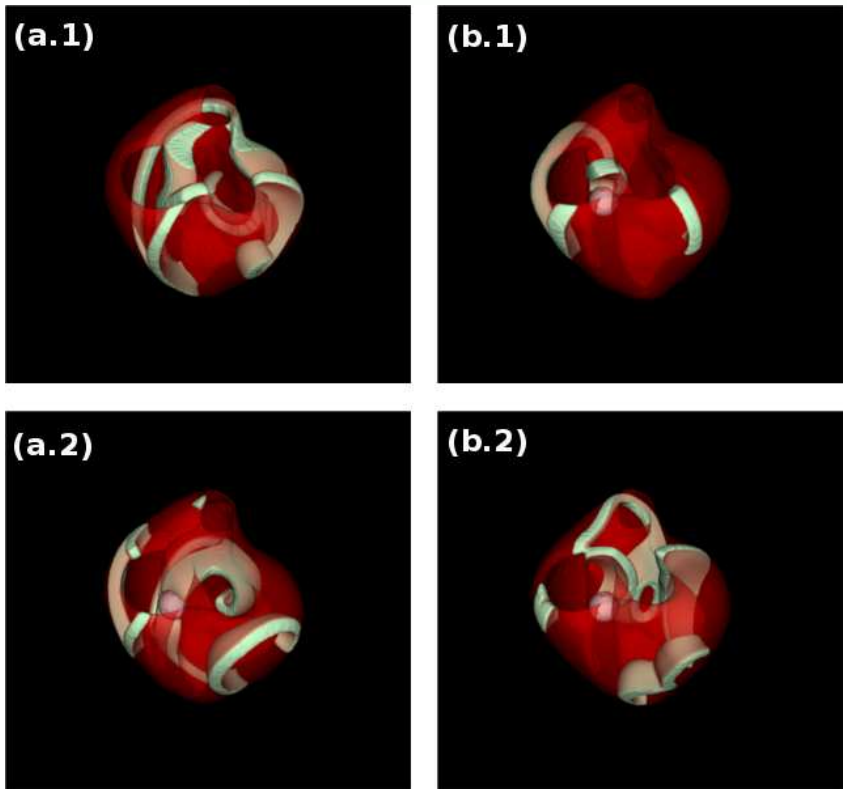

Spatiotemporal evolution of a scroll wave in an anatomically realistic domain (ventricles of a porcine heart) for the Panfilov model with a spherical obstacle of radius 2 mm: (a.1) and (a.2) scroll waves at t= 0.77 s and 4.35 s and ϵ_1= 0.05; (b.1) and (b.2) broken scroll waves at t= 0.77 s and 4.35 s and ϵ_1= 0.01.

Animations: Panfilov model

Square obstacle, VF
Square obstacle, VT
Square obstacle, NS
Two obstacles, VF
Two obstacles, VT
Two obstacles, NS
3D, ST
3D, RS
3D, NS
Scroll wave in anatomically realistic model, VT
Broken scroll wave in anatomically realistic model, VF
Spherical obstacle, VT
Spherical obstacle, VF

Animations: TNNP model

Square obstacle, VT
Square obstacle, RS
Square obstacle, NS
3D, FR anisotropy 30 degree
Scroll-wave,FR anisotropy 30 degree with cylindrical obstacle

Ionic Inhomogeneities

- How do ionic heterogeneities in cardiac tissue affect spiral-wave dynamics?
- Ionic heterogeneities can arise from ischemia, chronic heart failure or even from genetic disorders.
- They affect the APD and its timescales and thence the final state (periodic, quasiperiodic, or chaotic).

Ionic Inhomogeneities

Complex-periodic spiral waves in confluent cardiac cell cultures induced by localized inhomogeneities

Seong-min Hwang, Tae Yun Kim, and Kyoung J. Lee*

National Creative Research Initiative Center for Neuro-dynamics and Department of Physics, Korea University, Seoul 136-713, Korea

Edited by Harry L. Swinney, University of Texas, Austin, TX, and approved May 23, 2005 (received for review February 24, 2005)

Spatiotemporal wave activities in excitable heart tissues have long been the subject of numerous studies because they underlie

states are found to be common in this system. Analysis on their tip trajectory orbits suggest that there are many localized inho-

ϵ_1: Panfilov Model

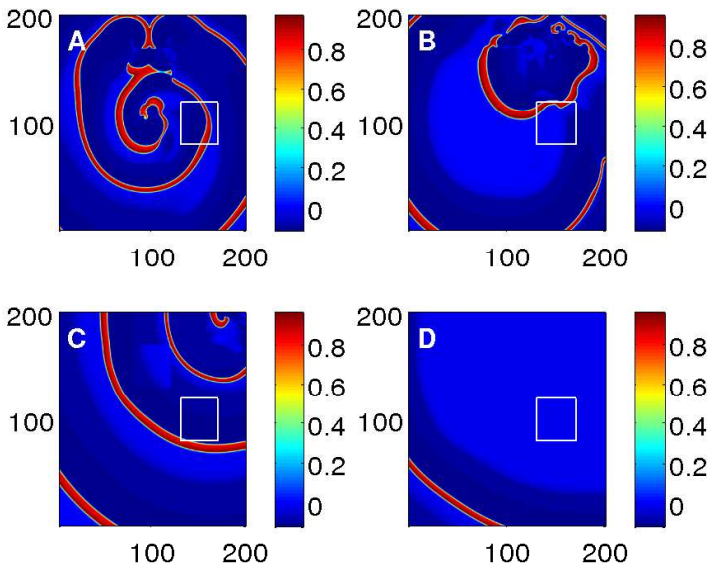

With ϵ_1^{out}=0.01 and ϵ_1^{in}=0.02 and an ihomogeneity placed at (130 mm, 80 mm) the spiral wave moves away from the medium: pseudocolour plots of V at 1100 ms (A), 1650 ms (B) and 2200 ms (C).

ϵ_1: Panfilov Model

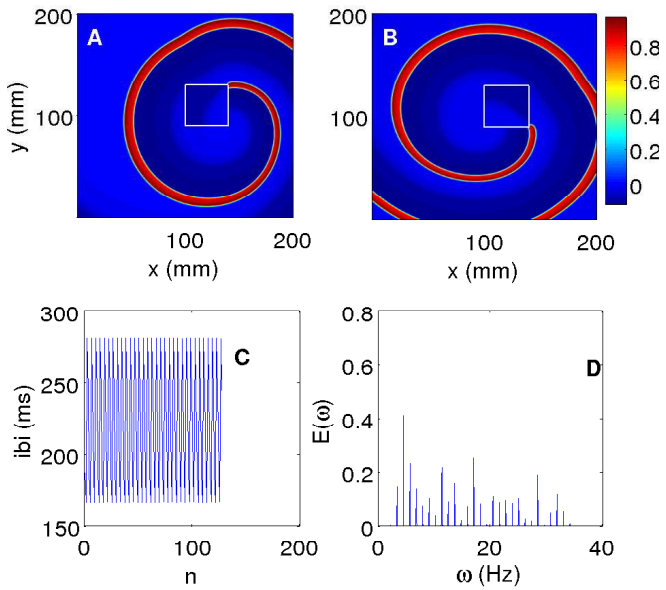

The spiral wave gets anchored to the inhomogeneity. Here ϵ_1^{out}=0.01 and ϵ_1^{in} = 0.02. The inhomogeneity is placed at (100 mm, 90 mm). Though the spiral gets anchored, its motion is quasiperiodic.

Ionic Inhomogeneities: TNNP

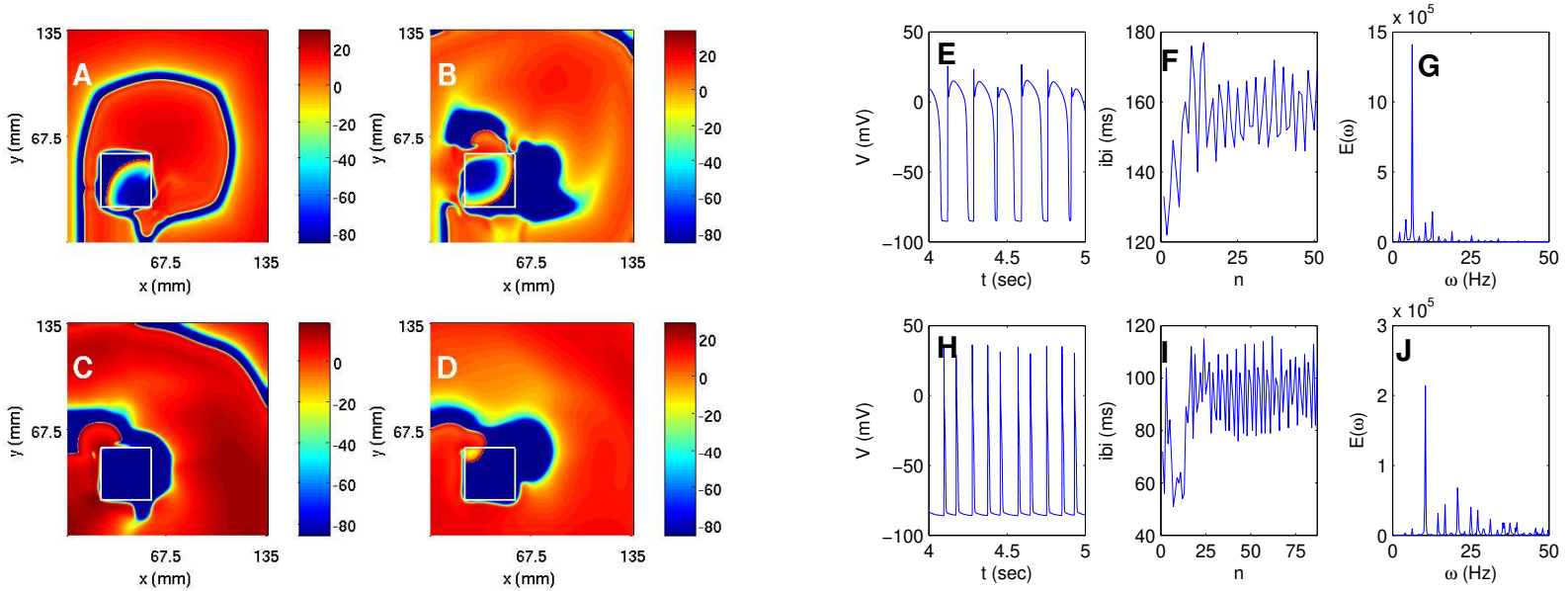

Different quasiperiodic motion observed inside and outside inhomogeneity with three underlying incommensurate frequencies in each case. Here the inhomogeneity of side $l = 33.75$ mm is placed at ($x = 22.5$ mm, $y = 22.5$ mm) with $G^{out}_{CaL} = 0.000175$ (maximal value) and $G^{in}_{CaL} = 0.00003$.

Ionic Inhomogeneities: 3D TNNP model

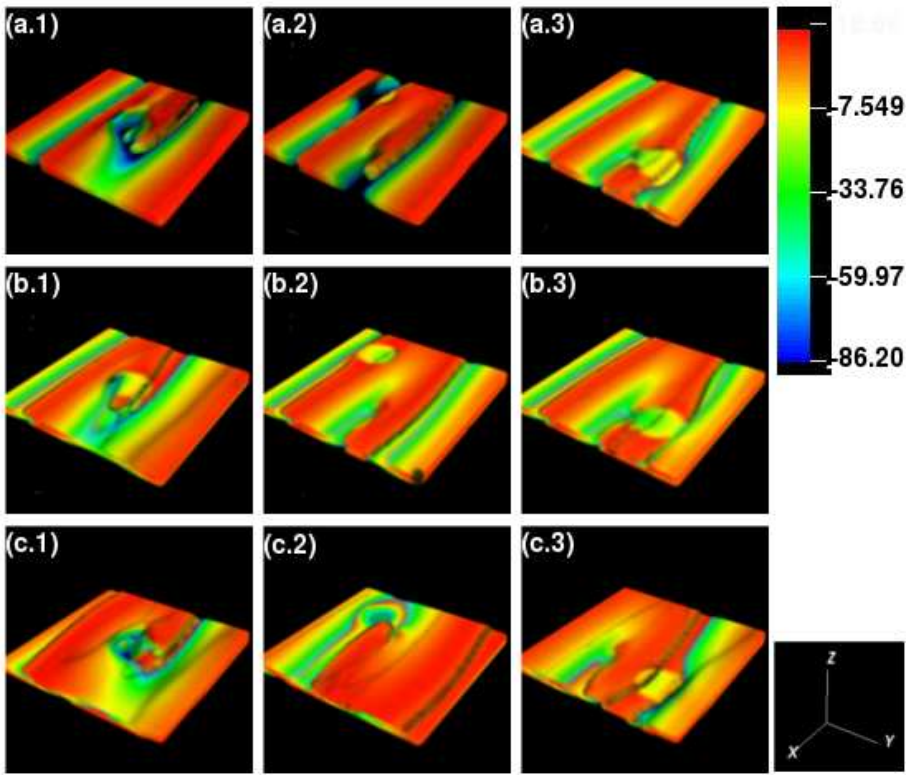

A comparison of the sensitive dependencies of scroll-wave dynamics in a slab of simulated human cardiac tissue under the coupled effect of FR (top to bottom) and cylindrical ionic-type inhomogeneities, for 3 different positions of the obstacle (left to right).

Local Control: No Obstacle

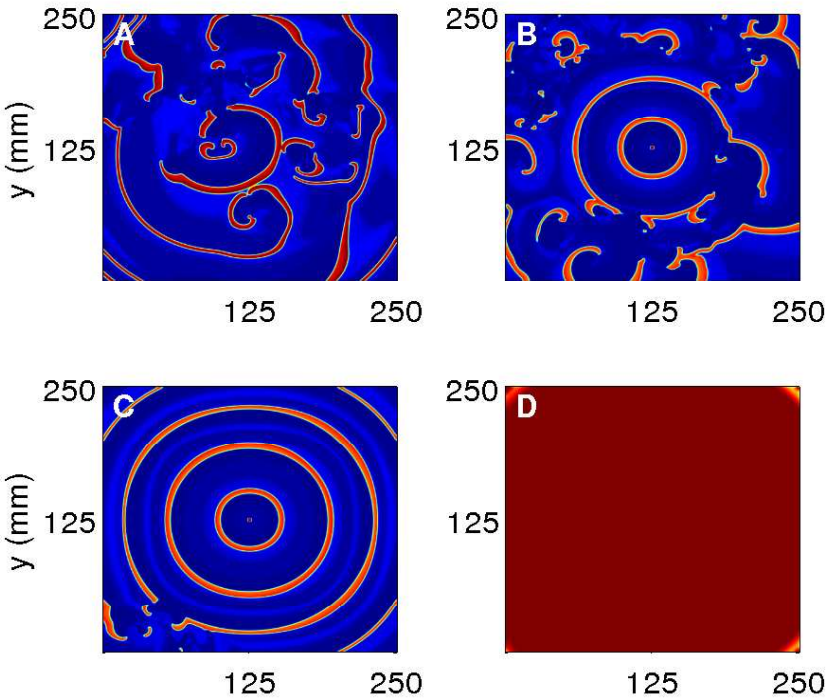

Elimination of spiral turbulence in Panfilov model by local periodic forcing, *Hu et al.* (2003)

Local Control: Obstacle

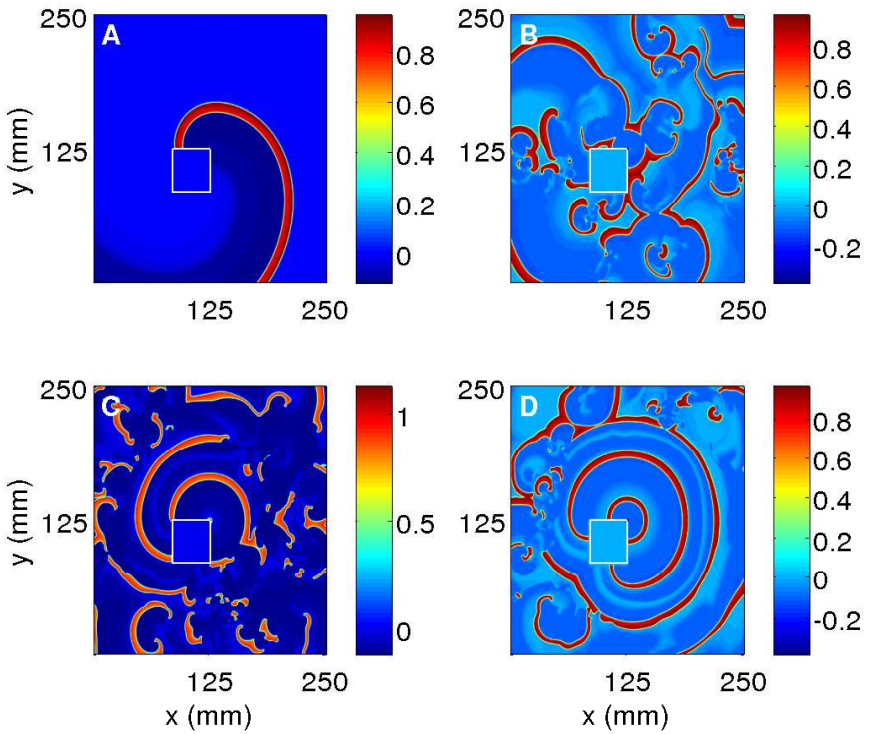

Unsuccessful to control spiral turbulence in Panfilov model with obstacle

Mesh-based Control: Obstacle

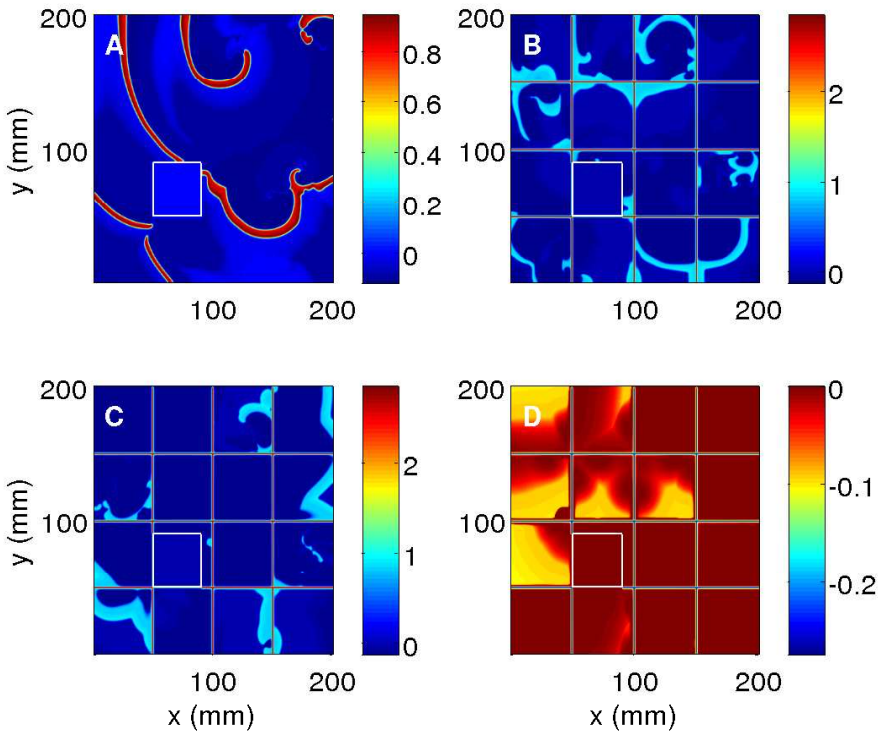

Successful to control spiral turbulence in Panfilov model by spatially extended mesh-based control scheme with obstacle

Control: TP06 model with inhomogeneity

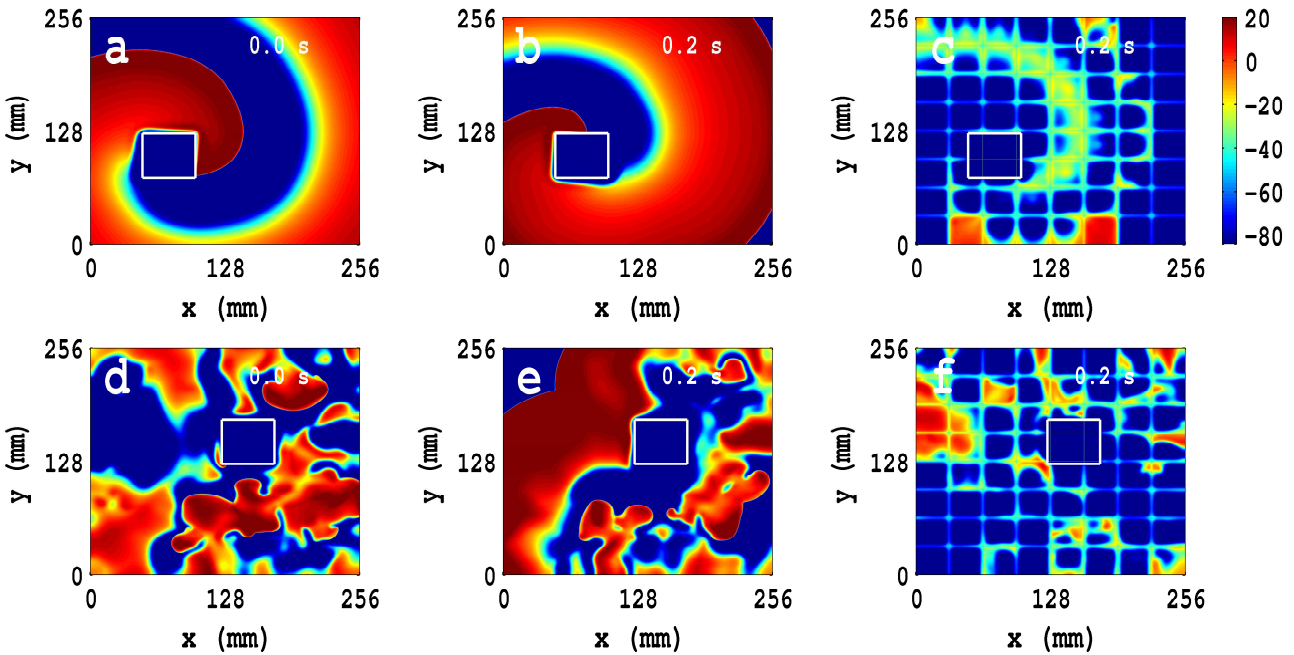

Animation

Spiral-wave control in the TP06 model in the presence of a square shape conduction inhomogeneity of size $\ell = 50$ mm by low-amplitude control pulses.

Fibroblast Inhomogeneities

- Fibroblasts are non-myocyte cells.
- Origin: enormous growth of such cells after a myocardial infarction.
- Experiment shows that they are not excitable.
- Fibroblasts can be modelled as RC circuits; they can also be coupled with myocytes via gap junctions.
- The precise values of the coupling constants are not known; but they must lie in a biophysically relevant range.

Myocyte-Fibroblast

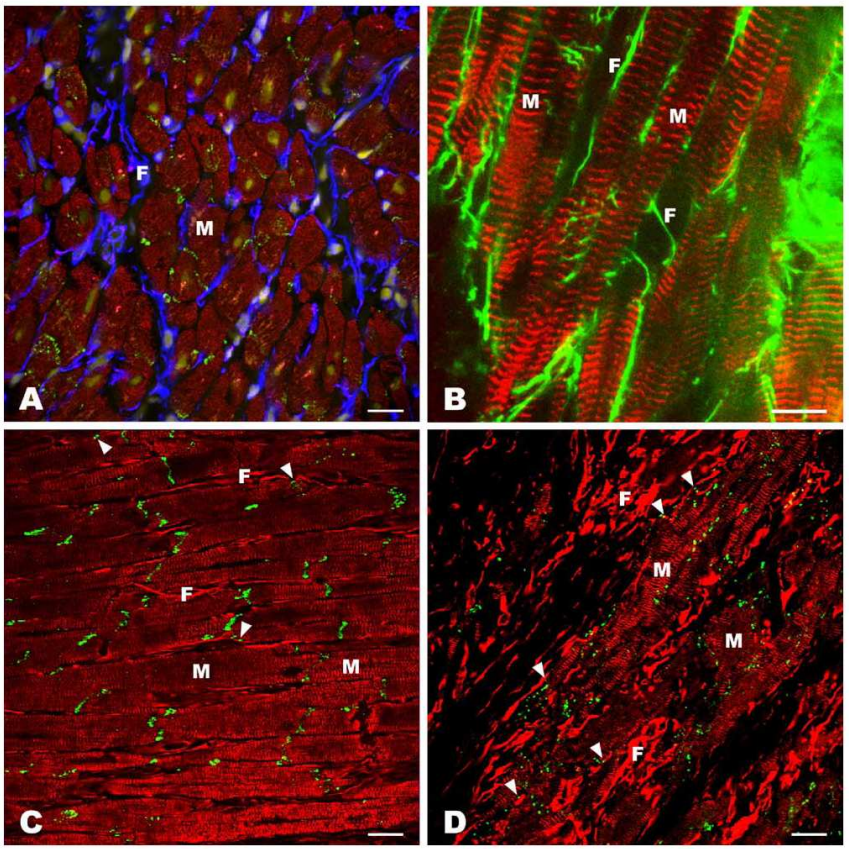

Fibroblast myocyte interrelation in the heart: (A,B) sheep ventricular myocardium; (C,D) rabbit ventricular myocardium. *Kohl et al. (2005), Journal of Electrocardiology.*

Model: An MF Composite

The model equation is:

$$C_{m,tot}\frac{\partial V_m}{\partial t} = -I_{ion,m} + \sum_{n}^{N_f} I_{gap,n},$$

$$C_{f,tot,n}\frac{\partial V_{f,n}}{\partial t} = -I_{ion,f_n} - I_{gap,n},$$

where

$$I_{ion,f} = G_f(V_f - E_f);$$
$$I_{gap,n} = G_{gap}(V_{f,n} - V_m).$$

G_f : fibroblast conductance (nS); E_f : fibroblast resting membrane potential (mV) ; G_{gap} : gap junctional conductance (nS).

Model: 2D tissue

- We model this in two ways:
  - Bilayer with each site has MF composites;
  - Monolayer of M cells with randomly distributed F cells.

MF composite Bilayer Model

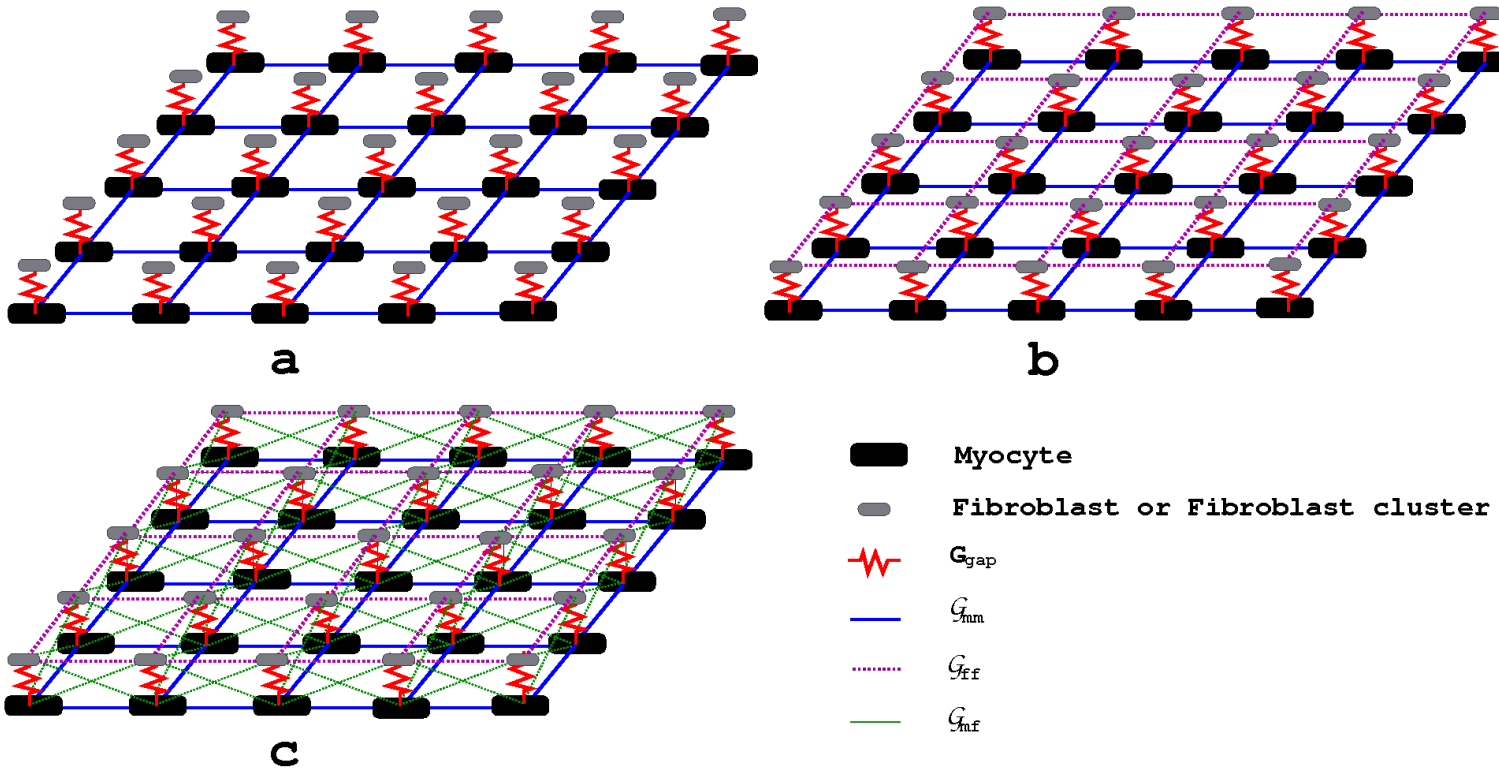

A schematic diagram of a small part of our square simulation domain with sites occupied by myocyte-fibrobalst (MF) composites, connected by G_{gap}, with (A) zero-sided, (B) single-sided, and (C) double-sided diffusive couplings between MF composites.

M-F Monolayer Model

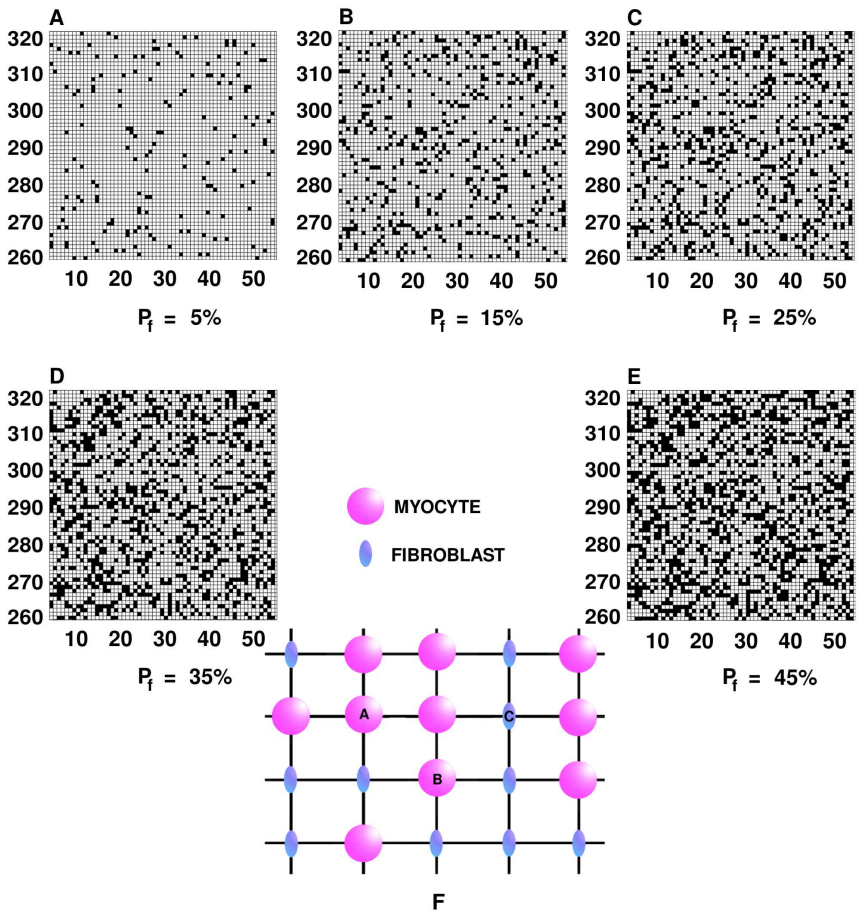

Spatial distributions of myocytes and fibroblasts in our simulation domain.

Model Parameters

- C_f: 6.3 to 75 pF
- G_f: 0.1 to 4 nS
- E_f: -50 to 0 mV
- G_{gap}: 0.3 to 8 nS

Refs: *Rook et al. (1992) Am J Physiol Cell Physiol, Kohl et al. (1994) Exp Physiol, Xie et al. (2009) Am J Physiol Heart Circ Physiol, Jacquemet et al. (2008) Am J Physiol Heart Circ Physiol,*

Homogeneous MF composites

Bilayer

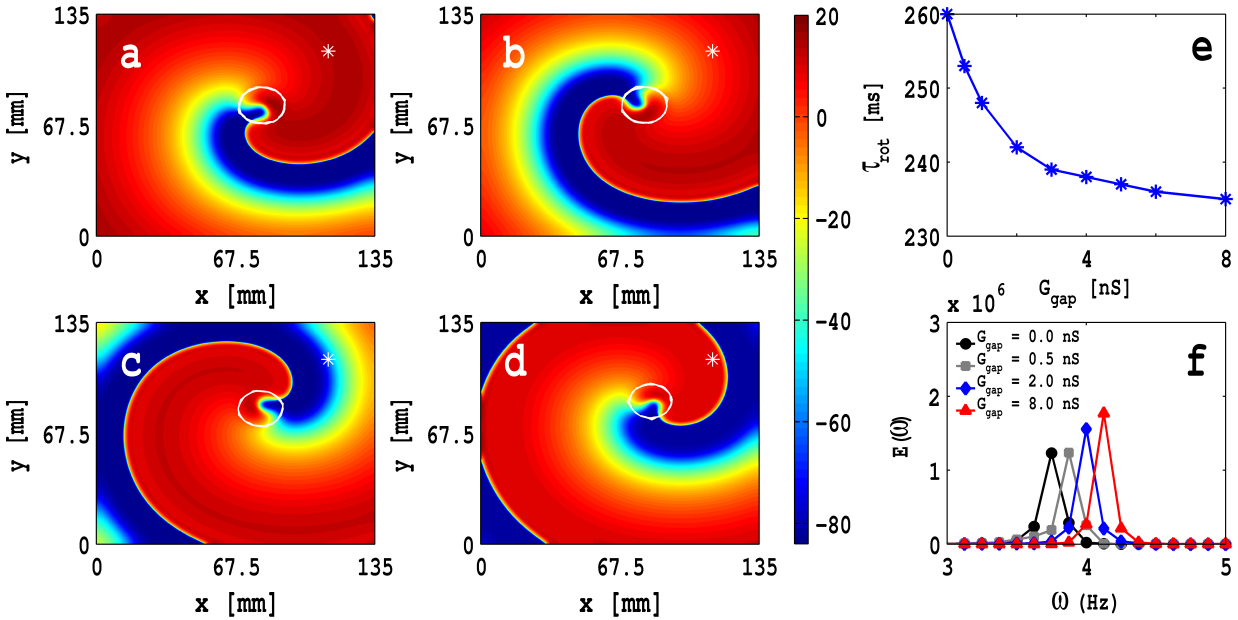

Pseudocolour plots of V_m, in a square simulation domain of side $L = 135$ mm, at time $t = 2$ s with $G_f = 4.0$ nS, $E_f = -39.0$ mV, zero-sided coupling with $D_{mm} = 0.00154$ cm^2/s, and (a) $G_{gap} = 0.0$ nS (control case, i.e., only myocytes), (b) $G_{gap} = 0.5$ nS (low coupling), (c) $G_{gap} = 2.0$ nS (intermediate coupling), and (d) $G_{gap} = 8.0$ nS (high coupling).

Homogeneous MF composites

Bilayer

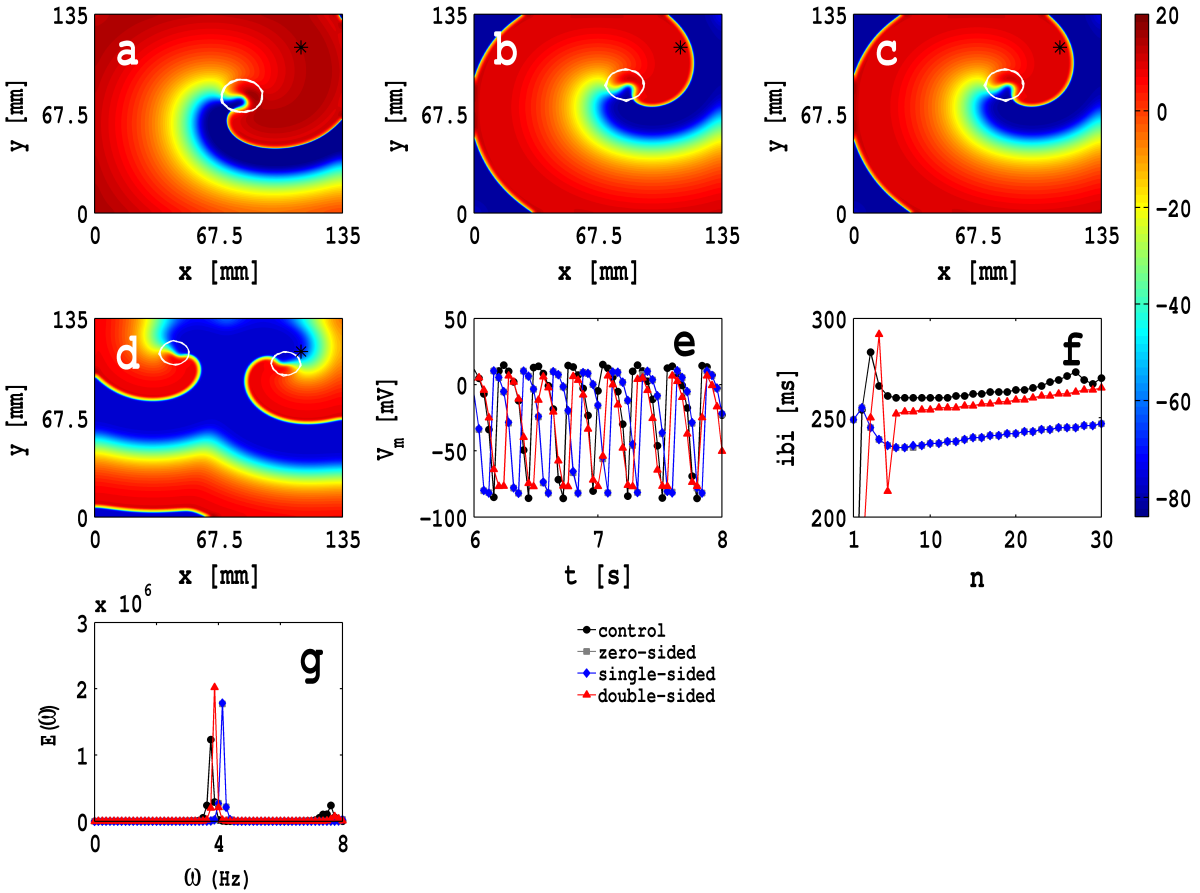

Spiral waves in pseudocolor plots of V_m at time $t = 2$ s in a simulation domain with $L = 13.5$ cm, an MF composite at every site, with a myocyte M coupled via $G_{gap} = 8$ nS with one fibroblast F ($C_{f,tot} = 6.3$ pF, $G_f = 4$ nS, and $E_f = -39$ mV) for (a) control case with only myocytes and no fibroblasts, (b) zero-sided coupling, (c) single-sided coupling with $\mathcal{G}_{mm}/\mathcal{G}_{ff} = 1$, and (d) double-sided coupling with $\mathcal{G}_{mm}/\mathcal{G}_{ff} = 1$ and $\mathcal{G}_{mm}/\mathcal{G}_{mf} = 200$.

Fibroblast Inhomogeneities: DS

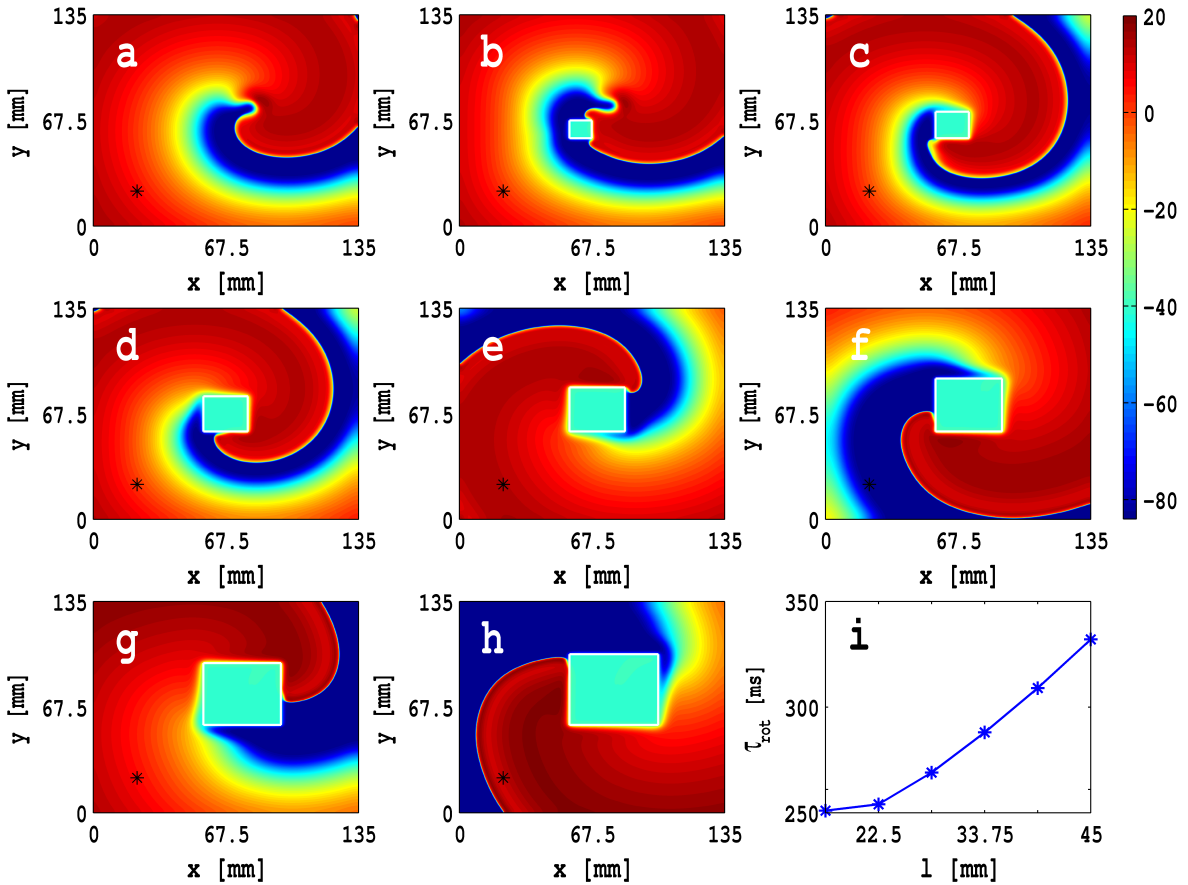

Animation

An MF-composite inhomogeneity can act like a conduction inhomogeneity.

Fibroblast Inhomogeneities: DS

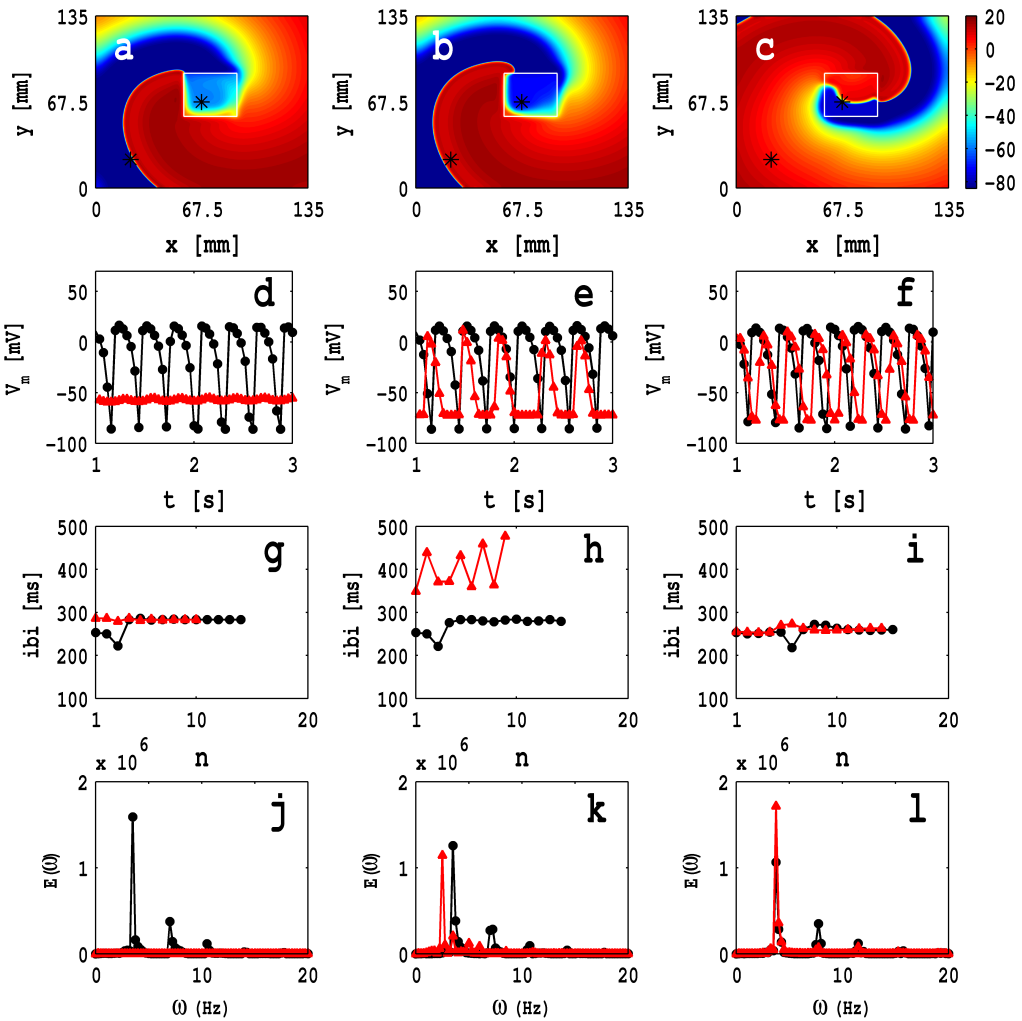

Animation

An MF-composite inhomogeneity can act like a ionic inhomogeneity.

Randomly distributed F: 2D Model

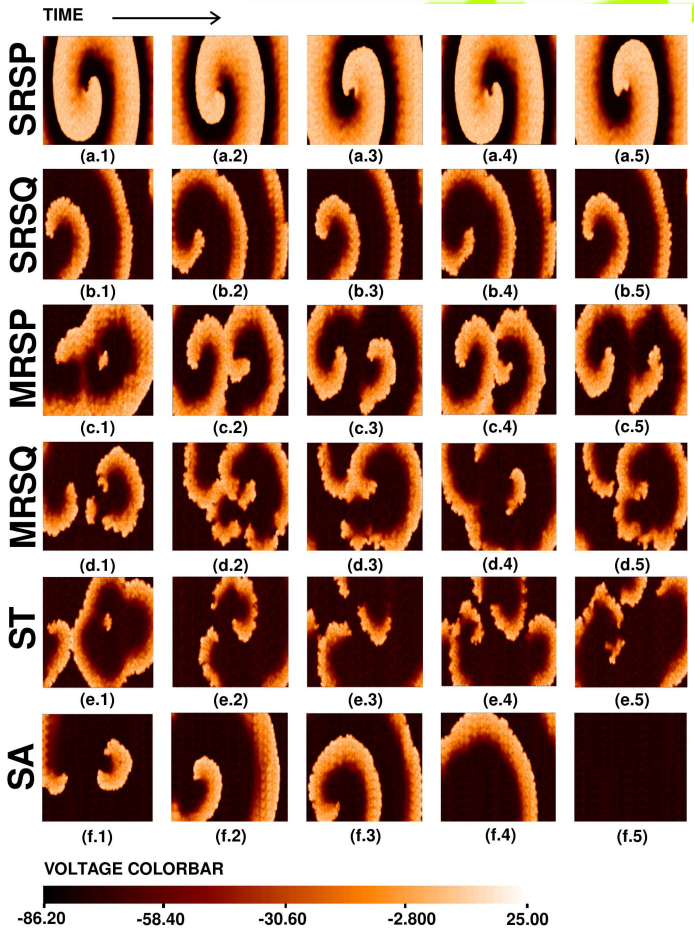

Animation

Pseudocolor plots of the local membrane potential V_m illustrating spiral-wave dynamics in a mural slice of our 2D simulation domain with a random distribution of myocytes and fibroblasts.

Randomly distributed F: 3D Model

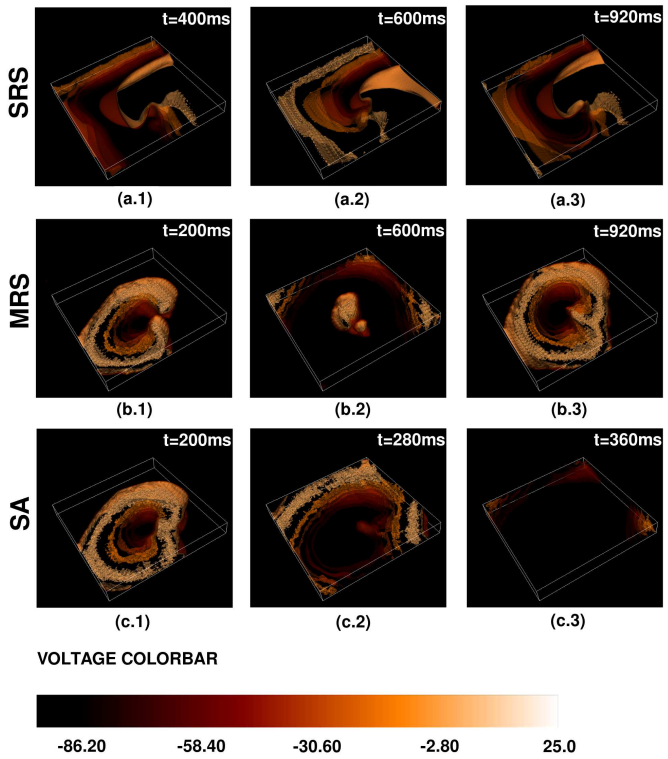

Animation

Pseudocolor isosurface plots of the local membrane potential V_m illustrating scroll-wave dynamics in a mural slice of our 3D simulation domain with a random distribution of myocytes and fibroblasts.

Randomly distributed Fibroblasts

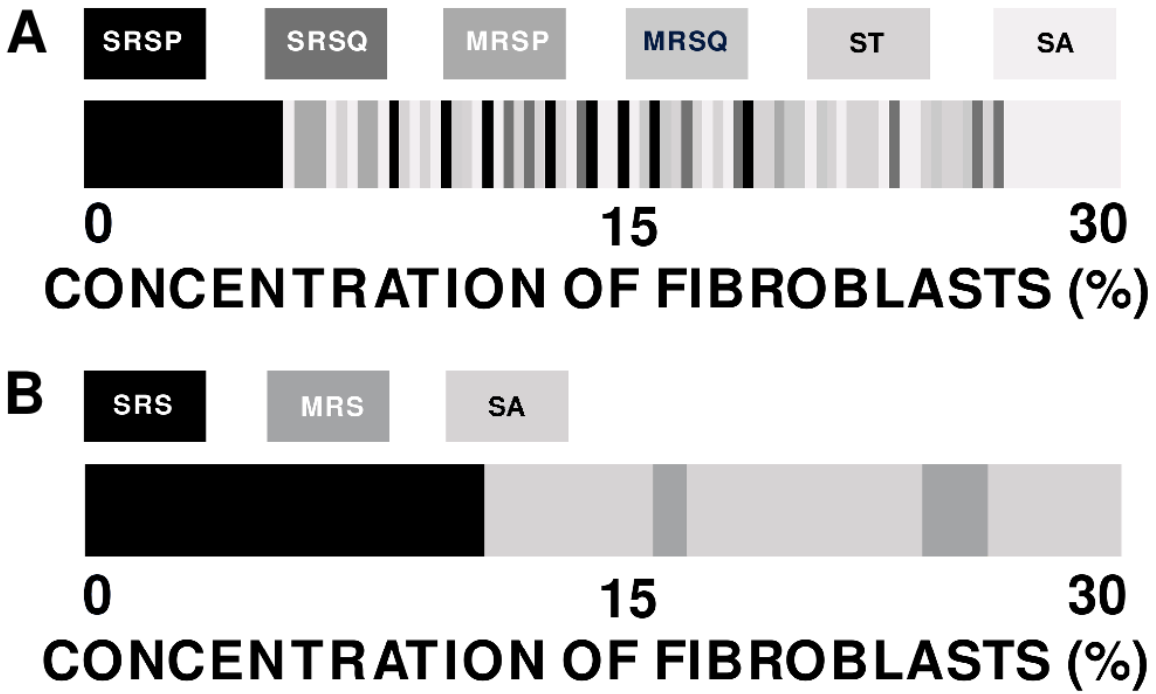

Representative band diagrams of states, in our 2D and in 3D studies, illustrating transitions between different spiral-wave (for 2D) and scroll-wave (for 3D) states as a function of P_f.

Control: An MF Inhomogeneity

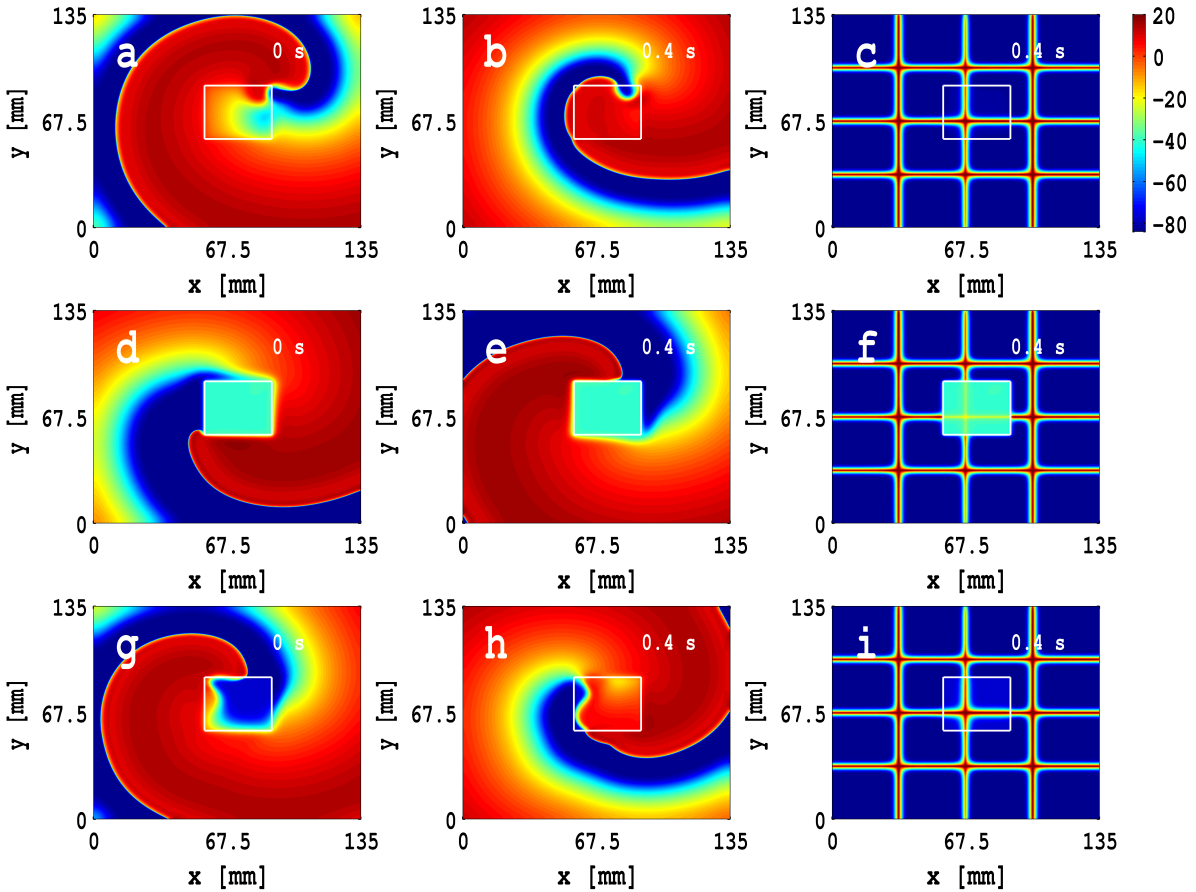

Animation

Spiral-wave control in the 2D Fibroblast model in the presence of a square shape MF composite inhomogeneity.

Mechanical Deformation

- Electrical activation leads to mechanical deformation (MD) of cardiac tissue.
- We use TP06 and TNNP04 model for our MD study.
- Any point $\mathbf{x} = (x, y)$ in the medium changes to $\mathbf{x}'(t) = (x'(t), y'(t))$ with

$$\begin{aligned} x'(t) &= x[1 + A_x(t)] \\ y'(t) &= y[1 + A_y(t)]. \end{aligned} \tag{8}$$

- We use a periodic MD with $A_x(t) = A_x \cos(\omega_x t)$ and $A_y(t) = A_y \cos(\omega_y t)$.

Plane wave CV

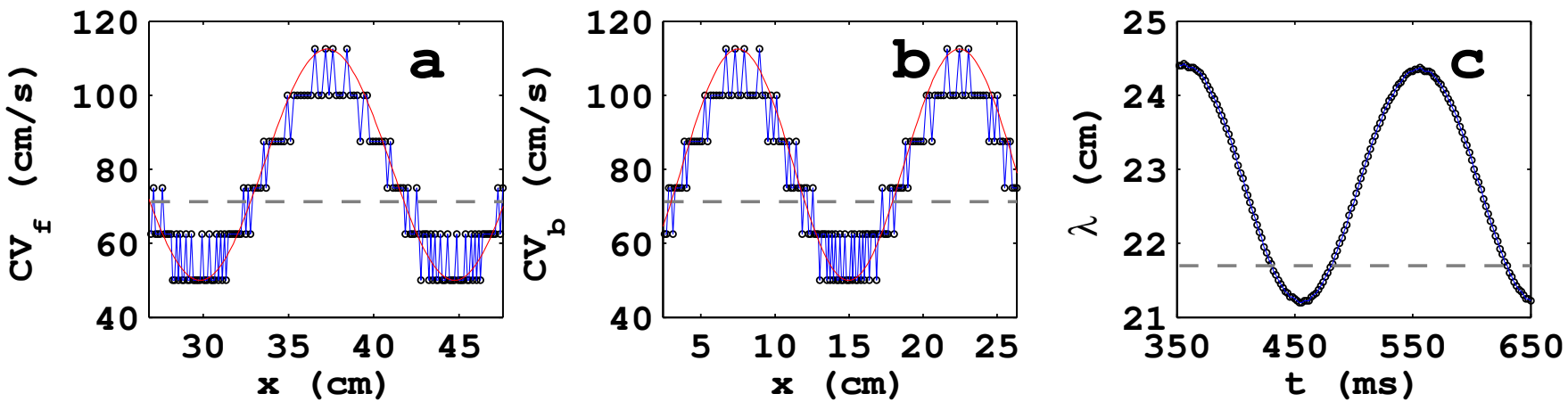

The modulation of the CV at wave-front and wave-back, and the wave length for a propagating wave in a deformed cable with amplitude $A_x = 0.75$ mm and frequency $f_x = 5.0\ \mathrm{s}^{-1}$ for the TP06 model.

Initial Configurations

- Three types of initial configurations.
- TP06 model: absence of deformation
  - IC1 leads to a rotating spiral state with a roughly circular spiral-tip trajectory (SRS).
  - IC2 leads to a single meandering spiral with turbulence (SMST).
  - IC3 leads to multiple-spiral turbulence (ST) with broken spiral waves.

ST states

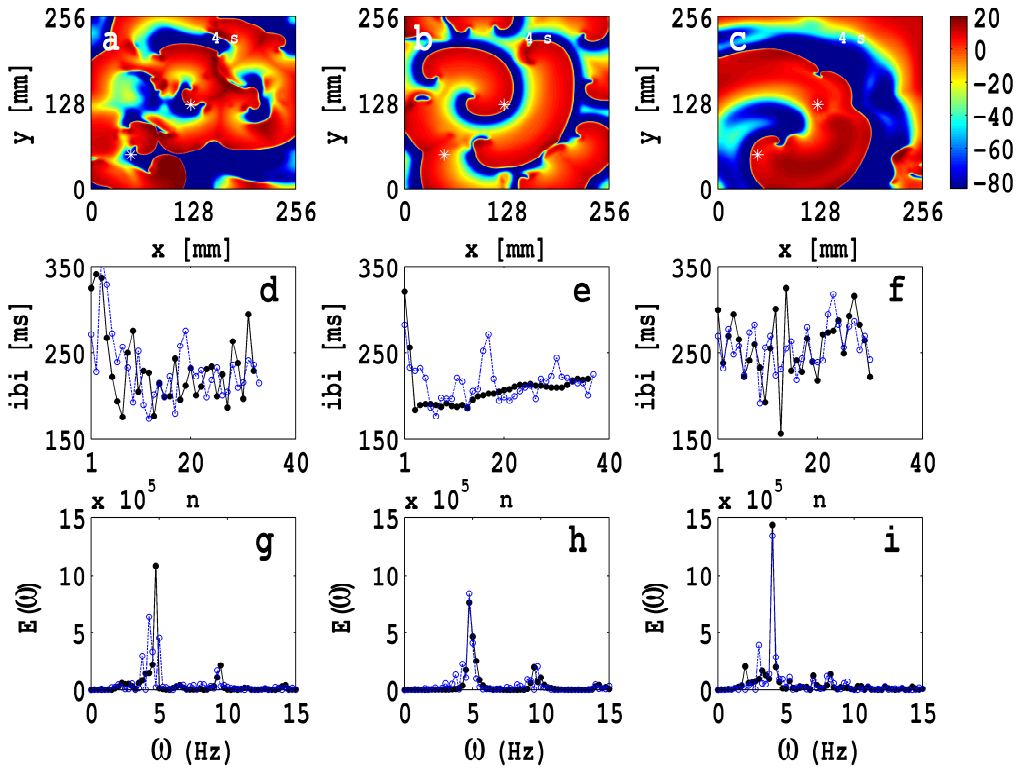

Pseudocolor plots of the transmembrane potential V_m for the TP06 model with MD along both $x-$ and $y-$axes with amplitudes and frequencies (a)$A_{x,y} = 0.075\ mm,\ f_{x,y} = 3.0\ s^{-1}$, (b) $A_{x,y} = 0.075\ mm,\ f_{x,y} = 5.0\ s^{-1}$, and (c) $A_{x,y} = 0.1\ mm,\ f_{x,y} = 7.0\ s^{-1}$.The animations (b3), (c3), and (d4) show the time evolution of these spiral waves in the interval $0 \leq t \leq 4\ s$. Animation

Control of Spiral turbulence

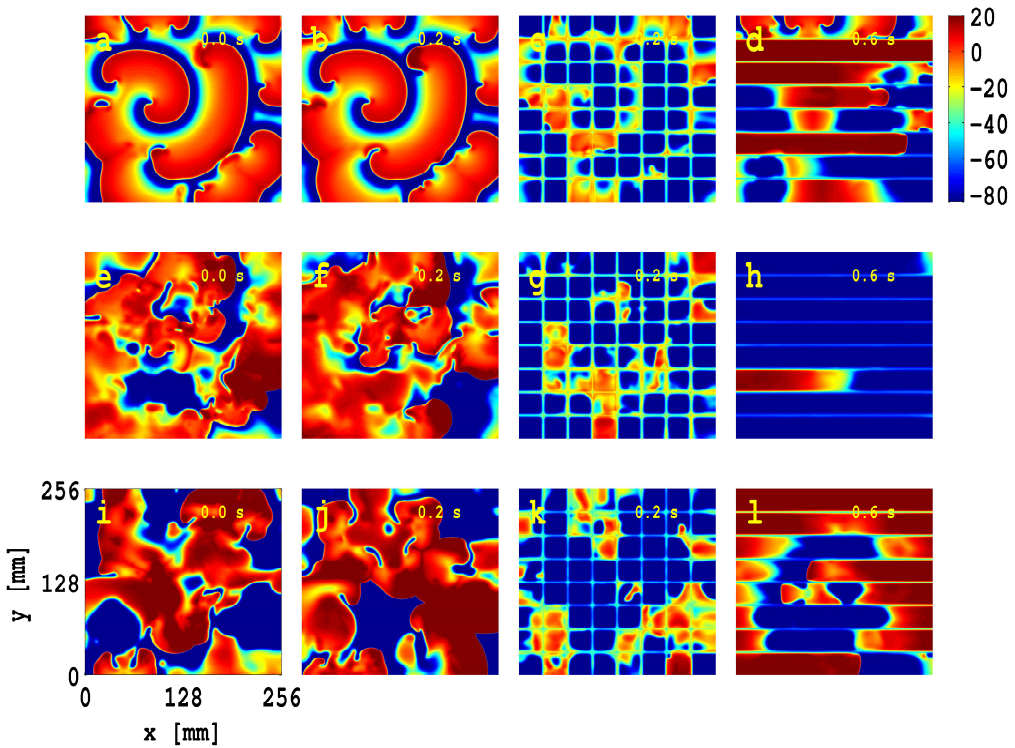

Spiral-wave control by low amplitude pulse in the TP06 model with MD along both x and y directions with amplitude $A = 0.075$ mm and frequency $f = 5$ Hz. Animation

Myocytes with Purkinje fibers

- Purkinje fibres are among the special conduction systems in cardiac tissue.
- They carry electrical impulses from *bundle of His* into the endocardium.
- Thus, electrical impulses excite the myocyte cells.
- These excitations propagate across ventricular tissue to develop the necessary amount of mechanical force to pump blood to the whole body.

Model: An EP composite

- An Endocardium-Purkinje (EP) composite can be modelled by:

$$\frac{\partial V_e}{\partial t} = -\frac{I_{ion,e}}{C_e} - \kappa(V_e - V_p) \quad (9)$$

$$\frac{\partial V_p}{\partial t} = -\frac{I_{ion,p}}{C_p} + \kappa(V_e - V_p) \quad (10)$$

where, $\kappa = D_{gap}/\Delta z^2$ decides the amount of flux that flows from the Purkinje to the endocardial cell via the heterocellular gap-junctional diffusion (at PVJ) D_{gap}

Model: 2D Purkinje Regular Network

The transmembrane potential of endocardium, V_e, and Purkinje, V_p for a 2D layer of cardiac simulation domain can be modelled by *discrete-reaction-diffusion* equations of the form:

$$\begin{bmatrix} \partial_t V_e(i,j) \\ \partial_t V_p(i,j) \end{bmatrix} = \begin{bmatrix} \frac{-I_{ion,e}(i,j)}{C_e} \\ \frac{-I_{ion,p}(i,j)}{C_p} \end{bmatrix} + \begin{bmatrix} D_{gap} & 0 \\ 0 & D_{gap} \end{bmatrix} \begin{bmatrix} \frac{V_p(i,j)-V_e(i,j)}{(\Delta z)^2} \\ \frac{V_e(i,j)-V_p(i,j)}{(\Delta z)^2} \end{bmatrix}$$

$$+ \begin{bmatrix} D_{ee} & 0 \\ 0 & D_{pp} \end{bmatrix} \begin{bmatrix} \frac{V_e(i+1,j)-2V_e(i,j)+V_e(i-1,j)}{(\Delta x)^2} + \frac{V_e(i,j+1)-2V_e(i,j)+V_e(i,j-1)}{(\Delta y)^2} \\ \frac{V_p(i+1,j)-2V_p(i,j)+V_p(i-1,j)}{(\Delta x)^2} + \frac{V_p(i,j+1)-2V_p(i,j)+V_p(i,j-1)}{(\Delta y)^2} \end{bmatrix} \quad (11)$$

here D_{ee} and D_{pp} represent, respectively, diffusion in the endocardium and Purkinje layers.

Model: 2D Purkinje structural Network

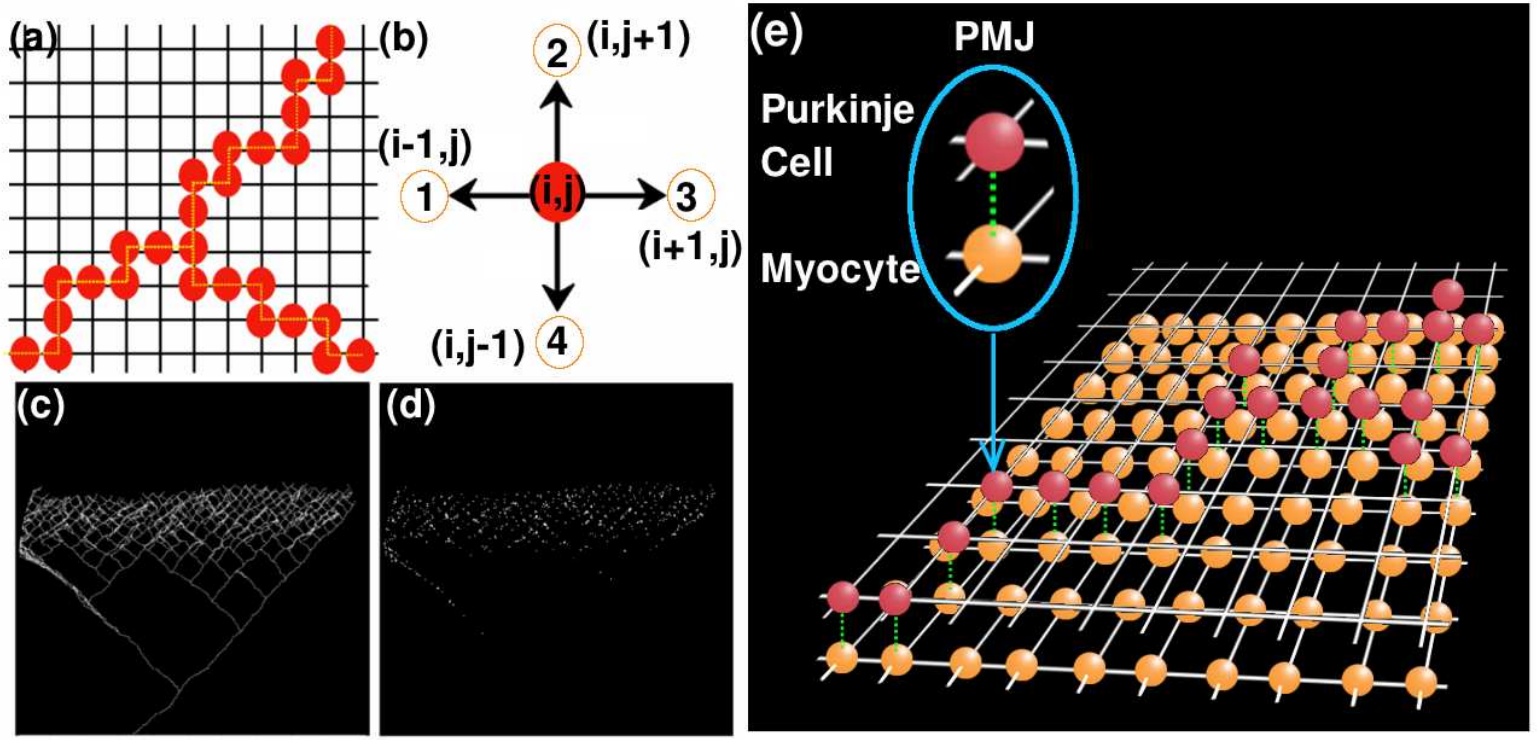

2D bilayer of EP composites

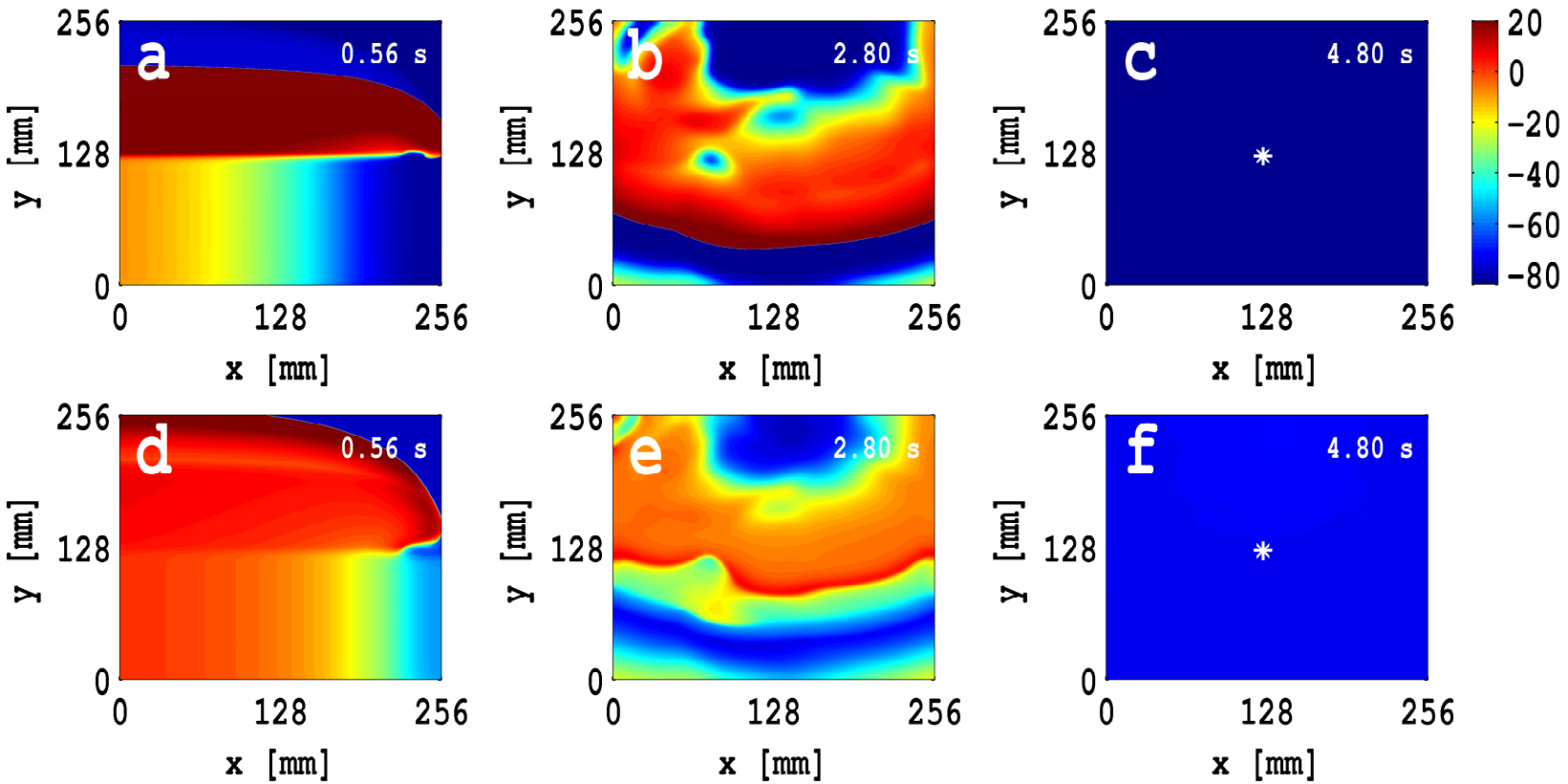

Initiation and evolution of spiral wave in a 2D bilayer of Purkinje and endocardium cells which has PVJ present at E:P=4:1.

2D bilayer of EP composites

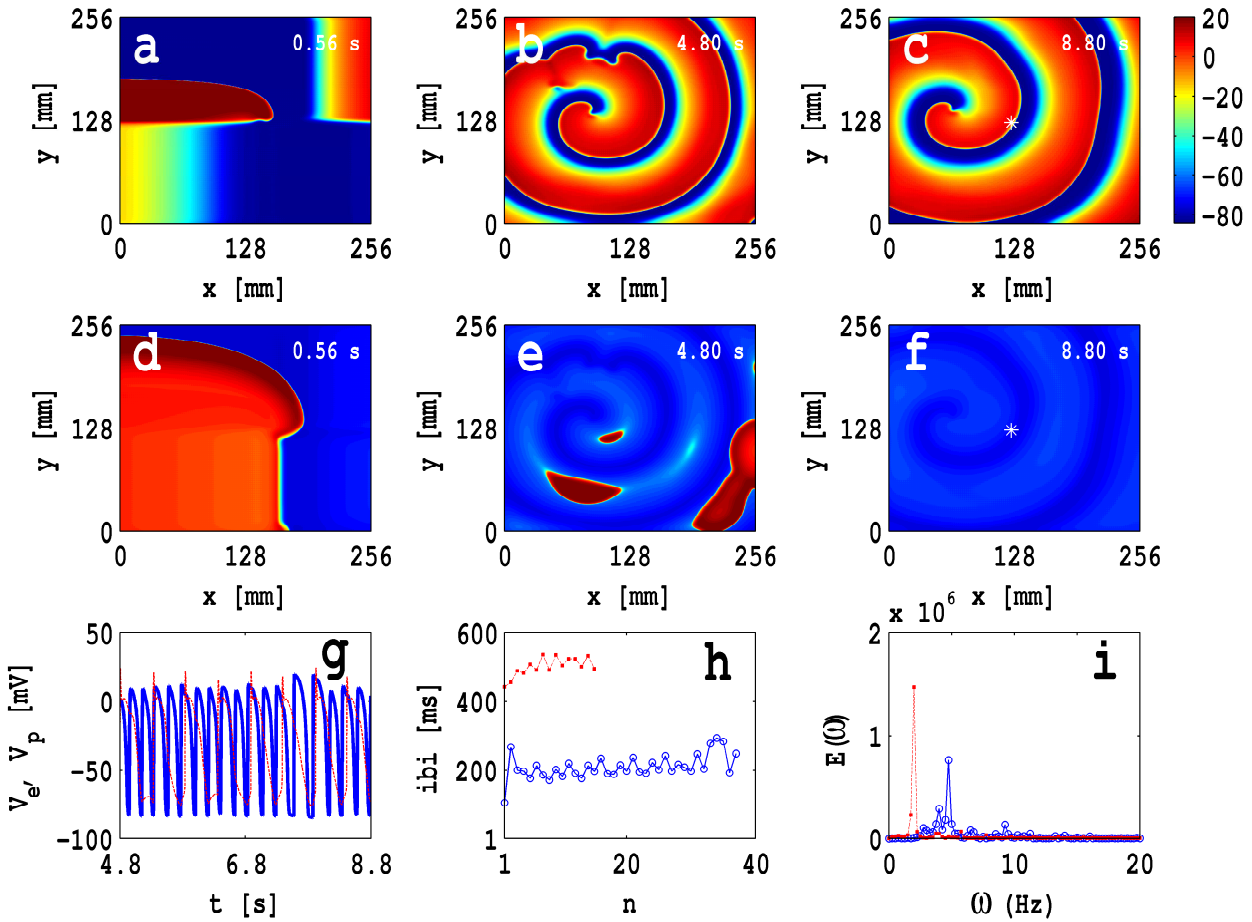

Initiation and evolution of spiral wave in a 2D bilayer of Purkinje and endocardium cells which has PVJ present at E:P=8:1.

Animations

A. Influence on SRS IC1
B. Influence on SMST IC2
C. Influence on ST IC3

2D Purkinje Network

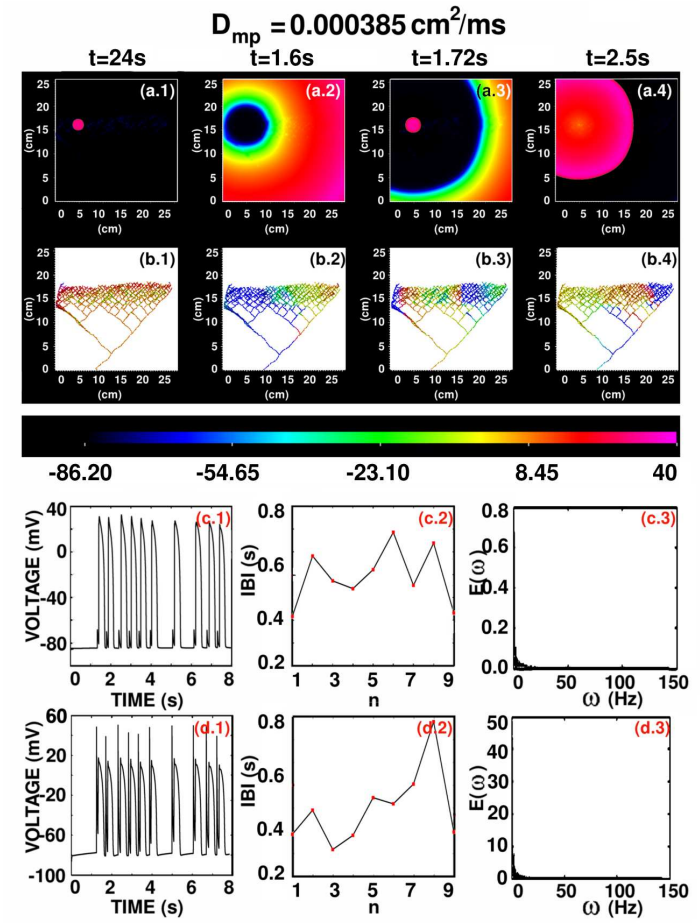

Signal propagation through His Purkinje system in the absence of external stimulus.

Purkinje Network: Influence on SRS

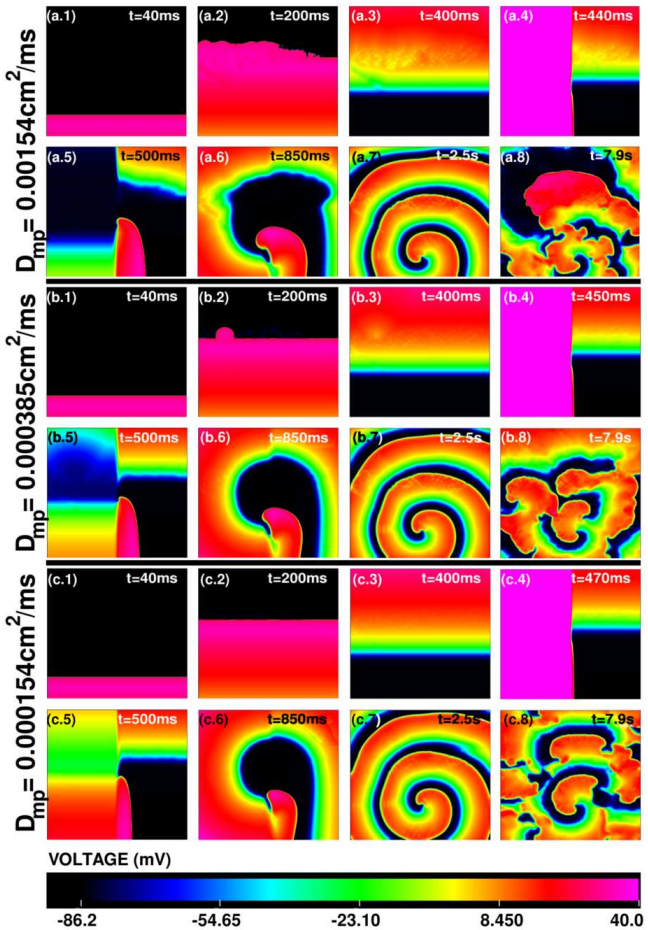

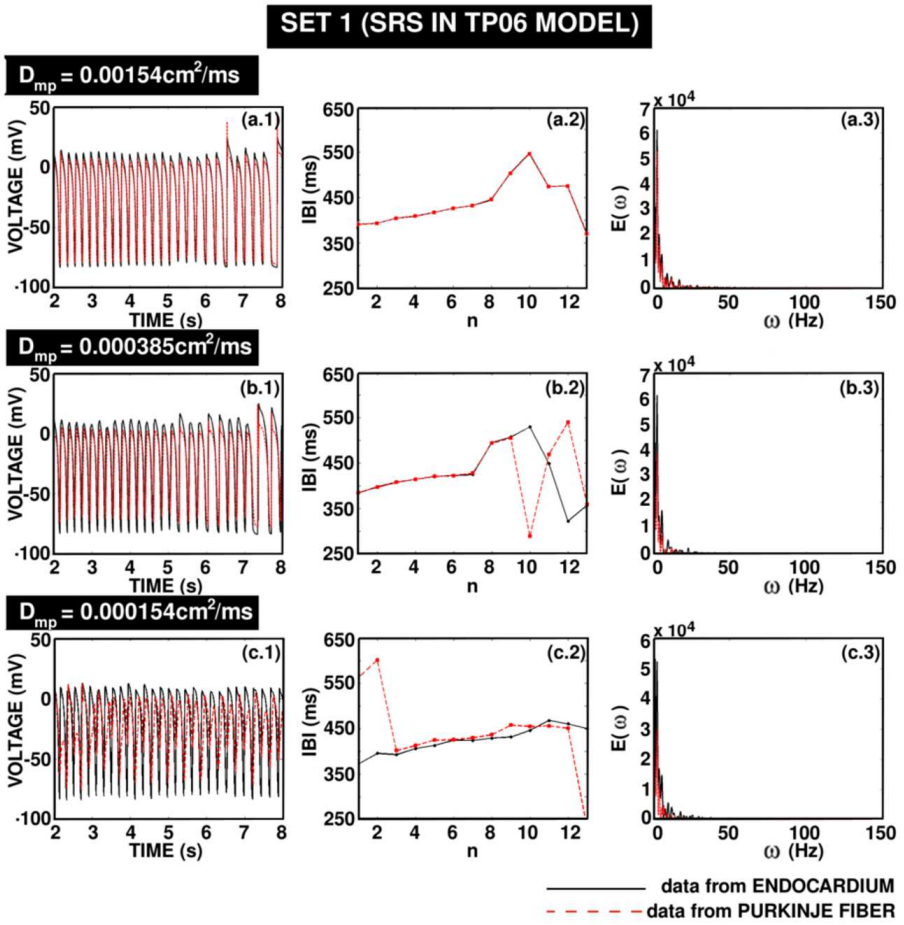

Animation

Purkinje Network: Influence on SMST

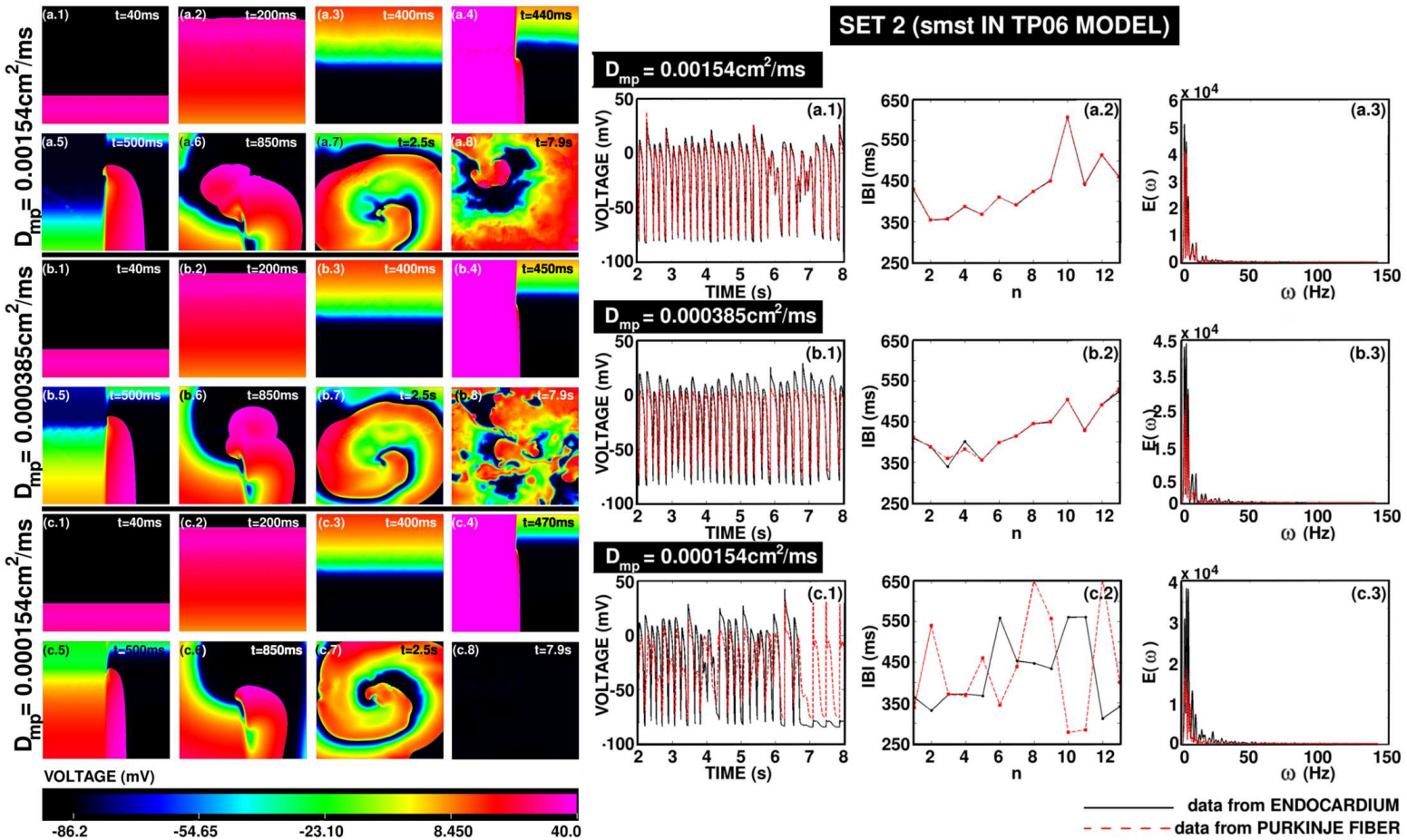

Animation

Purkinje Network: Influence on ST

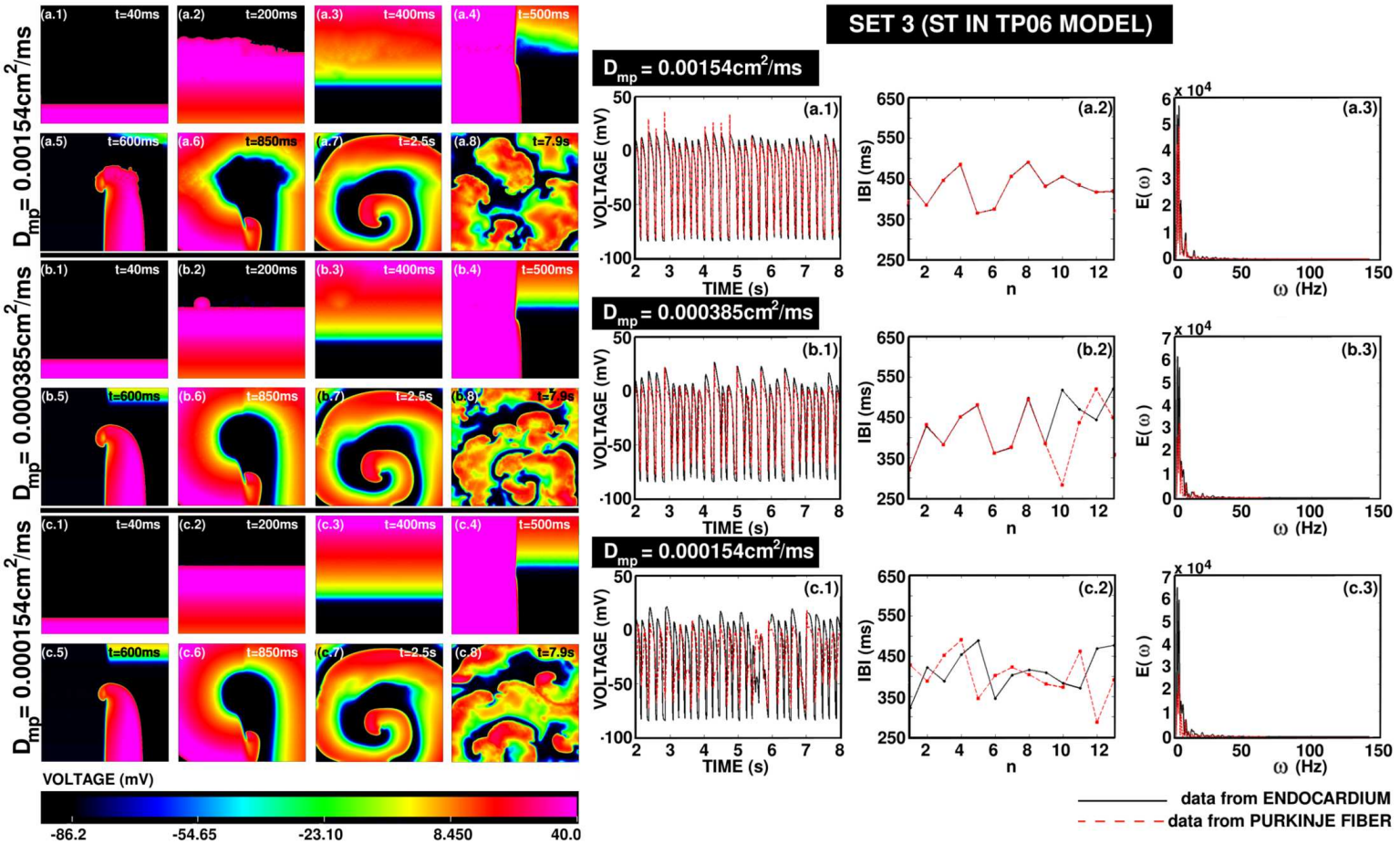

Animation

Purkinje Network: Scroll-wave Dynamics

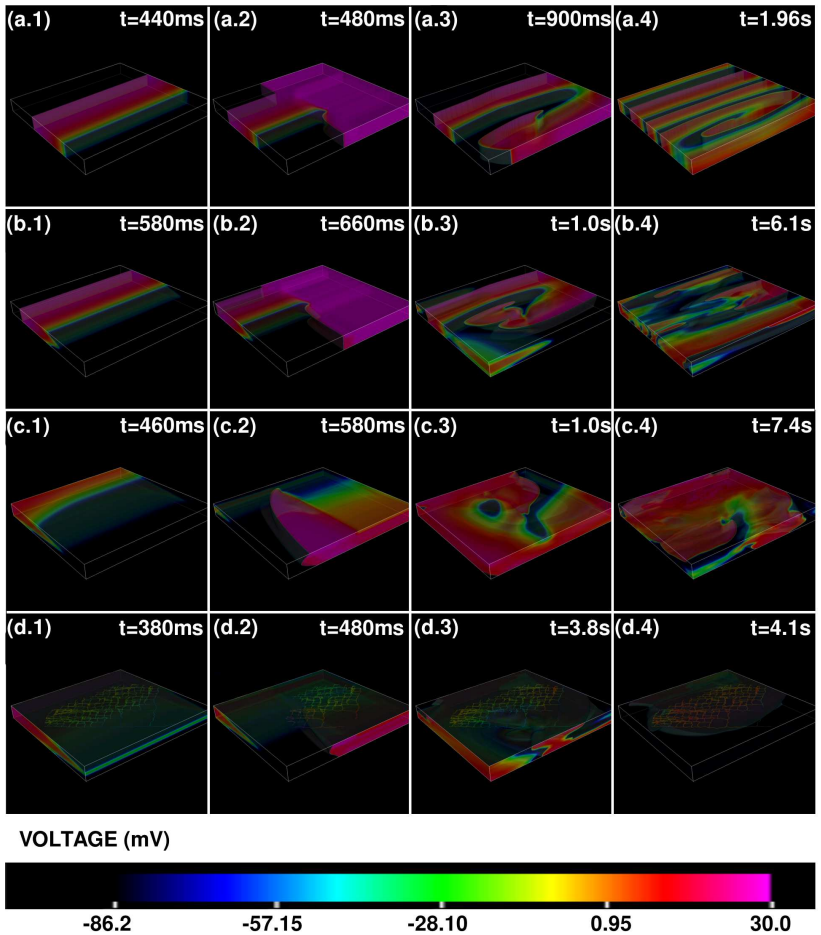

Animation

Control of Spiral Turbulence

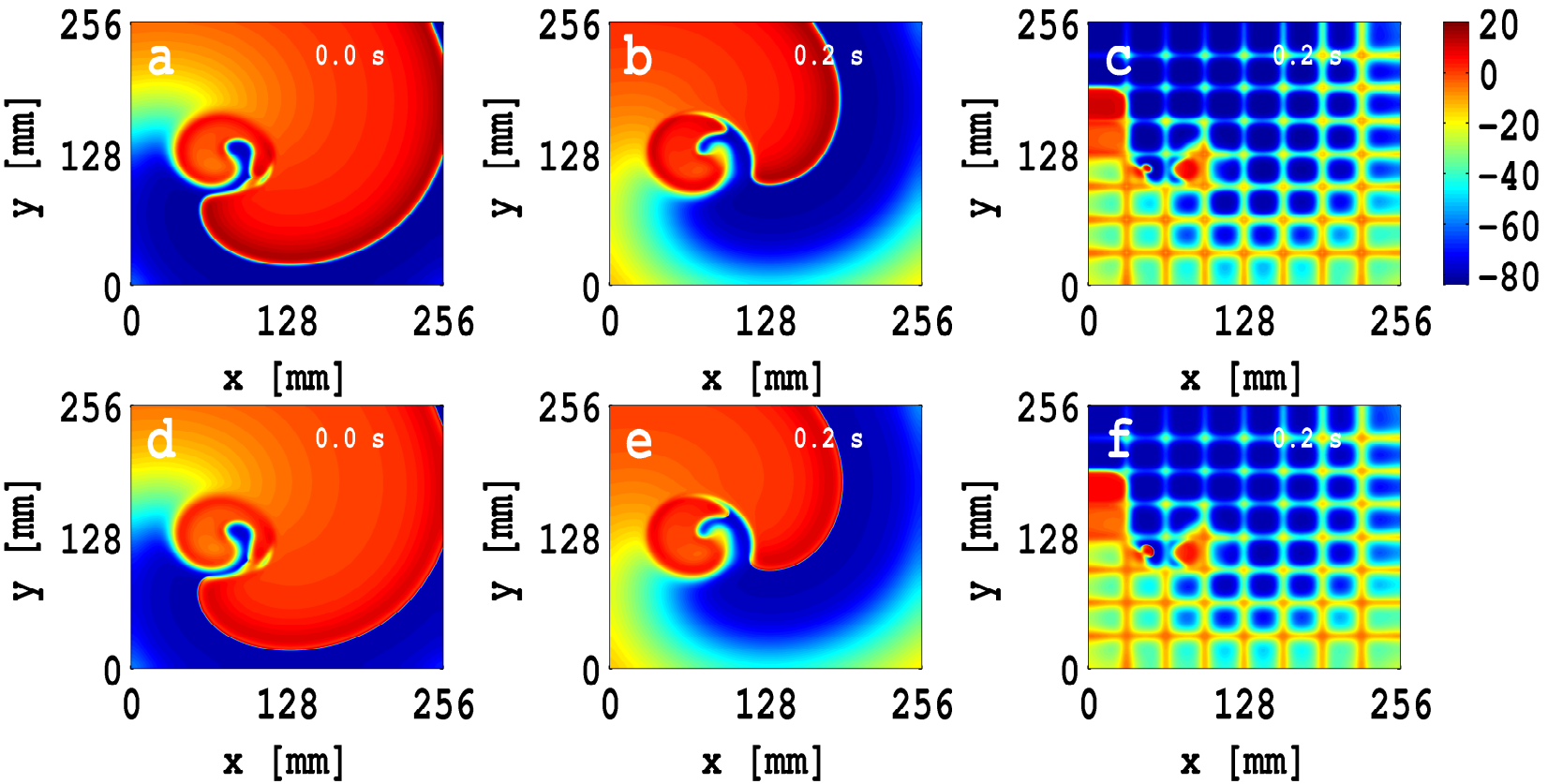

Control of spiral wave turbulence in both E and P layers by using our low-amplitude, mesh-based control scheme. Animation

Meandering Scroll Wave Dog Heart

Meandering Scroll-wave Dog-Heart Hund-Rudy Model. Animation

Broken Scroll Wave Dog Heart

Broken Scroll Wave Dog-Heart Hund-Rudy Model. Animation

Scroll Wave Human Heart

Scroll Wave Human-Heart TP06 Model. Animation

Broken Scroll Wave Human Heart

Broken Scroll Wave Human-Heart TP06 Model. Animation

Scroll-wave Breakup

Scroll-wave breakup because of a gradient in the fibroblast density in an anatomically realistic human-ventricular simulation domain. Animation

Scroll-wave Breakup

Scroll-wave breakup because of a gradient in the fibroblast density in an anatomically realistic human-ventricular simulation domain. Animation

Conclusions

- VF: breakup of spiral/scroll waves induced by reentrant activity.
- Spiral turbulence is a spatiotemporally chaotic phenomenon in models for cardiac tissue.
- The durations of chaotic transients depend on system size (small mammals are less likely to get heart attacks than large mammals).
- Spiral breakup in these models can be controlled by low-amplitude pulses.

Conclusions

- Our simulations show that cardiac arrhythmias depend sensitively on the shape, size, and positions of conduction inhomogeneities in ventricular tissue.
- This must arise because of a fractal boundary that separates the domain of attraction of VF from those of VT and quiescent behaviour.
- Our work provides a natural explanation for the large variety of experimental results.

Conclusions

- Ionic and timescale heterogeneities also result in spiral suppression, anchoring, and complex, spiral-wave dynamics.
- Like ionic inhomogeneities, fibroblast heterogeneities result in complex spiral- and scroll-wave dynamics.
- Optimal anti-tachycardia pacing and defibrillation protocols might well have to be tailor made for different patients (as is done already to some extent).
- Our control scheme works even with obstacles and a variety of inhomogeneities, etc., in contrast to local control schemes.

Thank You

Thank you for your attention.